

# 3

## Strength versus gravity

The existence of any differences of height on the Earth's surface is decisive evidence that the internal stress is not hydrostatic. If the Earth was liquid any elevation would spread out horizontally until it disappeared. The only departure of the surface from a spherical form would be the ellipticity; the outer surface would become a level surface, the ocean would cover it to a uniform depth, and that would be the end of us. The fact that we are here implies that the stress departs appreciably from being hydrostatic; ...

H. Jeffreys, *Earthquakes and Mountains* (1935)

### 3.1 Topography and stress

Sir Harold Jeffreys (1891–1989), one of the leading geophysicists of the early twentieth century, was fascinated (one might almost say obsessed) with the strength necessary to support the observed topographic relief on the Earth and Moon. Through several books and numerous papers he made quantitative estimates of the strength of the Earth's interior and compared the results of those estimates to the strength of common rocks.

Jeffreys was not the only earth scientist who grasped the fundamental importance of rock strength. Almost fifty years before Jeffreys, American geologist G. K. Gilbert (1843–1918) wrote in a similar vein:

If the Earth possessed no rigidity, its materials would arrange themselves in accordance with the laws of hydrostatic equilibrium. The matter specifically heaviest would assume the lowest position, and there would be a graduation upward to the matter specifically lightest, which would constitute the entire surface. The surface would be regularly ellipsoidal, and would be completely covered by the ocean. Elevations and depressions, mountains and valleys, continents and ocean basins, are rendered possible by the property of rigidity.

G. K. Gilbert, *Lake Bonneville* (1890)

By *rigidity* Gilbert meant the resistance of an elastic body to a change of shape. He was well aware that this *rigidity* has its limits, and that when some threshold is exceeded Earth materials fail to support any further loads. We call this threshold *strength* and recognize that this material property resists the tendency of gravitational forces to erase all topographic variation on the surface of the Earth and the other solid planets and moons.

The importance of strength is highlighted by a simple computation that Jeffreys included in his masterwork, *The Earth* (1952). This computation is summarized in Box 3.1, where it is shown that, without strength, a topographic feature of breadth  $w$  would disappear from the surface of a planet in a time  $t_{\text{collapse}}$  given by:

$$t_{\text{collapse}} = \sqrt{\frac{\pi w}{8g}} \quad (3.1)$$

where  $g$  is surface gravitational acceleration. Without strength, a mountain 10 km wide on the Earth would collapse in about 20 seconds, and a 100 km wide crater on the moon would disappear in about 3 minutes. Clearly, such features can and do persist for much longer periods of time.

Planetary topography, and the material strength that makes it possible, lend interest and variety to planetary surfaces. However, when seen from a distance, it is clear that the shapes of planets are, nevertheless, very close to spheroids. Only very small asteroids and moons (Phobos and Deimos are examples) depart greatly from a spheroidal shape in equilibrium with their rotation or tidal distortion. Thus, although the strength of planetary materials (rock or ice) is adequate to support a certain amount of topography, it is evidently limited. Such things as 100 km high mountains do not exist on the Earth because strength has limits. The ultimate extremes of altitude on a planet's surface are regulated by the antagonism between the strength of its surface materials and its gravitational field.

Although everyone has an intuitive idea of *strength*, the full quantification of this property is both complex and subtle. Many introductory physics or engineering textbooks present strength as if it were a simple number that can be looked up in the appropriate handbook. This impression is reinforced by handbooks that offer tables of numbers purporting to represent the *strength* of given materials. But further investigation soon reveals that there are different kinds of strength: crushing strength, tensile strength, shear strength, and many others. Strength sometimes seems to depend on the way that forces or loads are applied to the material, and upon other conditions such as pressure, temperature, and even its history of deformation. The various strengths of ductile metals, like iron or aluminum, typically do not depend much on how the load is applied, or how fast it is applied, but common planetary materials behave quite differently.

Quantitative understanding of the relation between topography, strength, and gravity requires, first, some elementary notions of stress and strain and, second, a more detailed understanding of how apparently solid materials resist changes in shape. This chapter introduces the basic concepts of stress, strain, and strength before failure, and applies them to the limits on possible topography. It also introduces the role of time and temperature in limiting the strength of materials and the duration of topographic features. The next chapter examines deformation beyond the strength limit and the tectonic landforms that develop when this limit is exceeded.

### Box 3.1 Collapse of topography on a strengthless planet

Consider a long mountain ridge of height  $h$ , width  $w$  and effectively infinite length  $L$  standing on a wide, level plain. For simplicity suppose that the profile of the mountain is rectangular, with vertical cliffs of height  $h$  bounding both sides (Figure B3.1.1). The surface gravitational acceleration of the planet on which this mountain lies is  $g$ , and  $\rho$  is the density of the material from which both the mountain and planetary surface are composed.

The weight of the mountain is  $\rho ghwL$ . If there is no strength, this weight (force) can only be balanced by the inertial resistance of material accelerating beneath the surface, according to Newton's law  $F = ma$ . The driving force  $F$  equals the weight of the mountain,  $F = \rho ghwL$ . The acceleration  $a$  is equal to the second time derivative of the mountain height,  $a = \frac{d^2h}{dt^2}$ . The mass being accelerated is less easy to compute exactly, but it is approximately the mass enclosed in a half cylinder of radius  $w/2$  beneath the mountain (this neglects the mass of the mountain itself, which is not strictly correct, but if  $h$  is small compared to  $w$ , the mountain mass is only a small correction). The mass is then  $m \approx \frac{\pi}{8} w^2 L \rho$ . This yields a simple, second-order differential equation for the mountain height  $h$  as a function of time,  $t$ :

$$\frac{d^2h(t)}{dt^2} = \frac{8}{\pi} \frac{g}{w} h(t). \quad (\text{B3.1.1})$$

This equation has the solution

$$h(t) = h_0 e^{-t/t_{\text{collapse}}} \quad (\text{B3.1.2})$$

where  $h_0$  is the initial height of the mountain and the timescale for collapse is given by:

$$t_{\text{collapse}} = \sqrt{\frac{\pi w}{8 g}}. \quad (\text{B3.1.3})$$

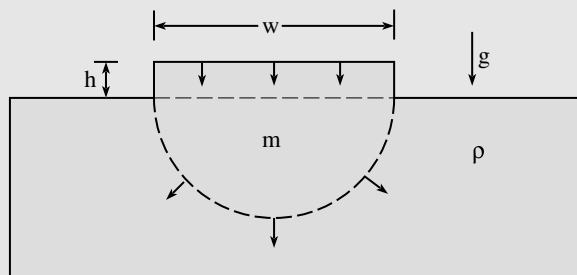


Figure B3.1.1 The dimensions and velocity of a linear collapsing mountain of height  $h$  and width  $w$  on a strengthless half space of density  $\rho$  that is compressed by the surface gravity  $g$  on a fluid planet. As the mountain collapses vertically it drives a plug of material of mass  $m$  underneath it that flows out through the dashed cylindrical surface.

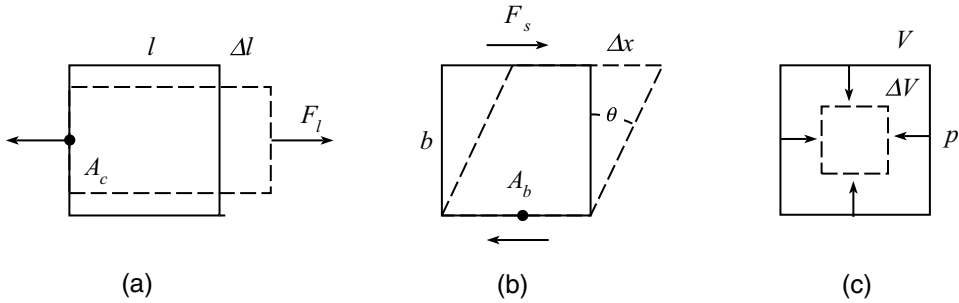


Figure 3.1 Three varieties of strain. (a) Longitudinal strain, in which a block of material of original length  $l$  and basal area  $A_c$  is extended an amount  $\Delta l$  by a force  $F_l$ . (b) Shear strain, in which the top of a block of height  $b$  is sheared a distance  $\Delta x$  relative to its base (to an angle  $\theta$ ) by a differential force  $F_s$ . (c) Volume strain, in which a block of original volume  $V$  is compressed an amount  $\Delta V$  by a pressure  $p$ .

### 3.2 Stress and strain: a primer

A full exposition of the continuum theory of stress and strain is beyond the scope of this book. For the intimate details, the reader is referred to sources such as Turcotte and Schubert's excellent book *Geodynamics* (2002). A few simple concepts will suffice for a general understanding of planetary surface processes, although the actual computation of stresses under the different loading conditions illustrated later in this chapter requires an application of the full theory of elasticity.

#### 3.2.1 Strain

Strain is a dimensionless measure of deformation. It is a purely geometric concept that is meaningful only in the limit where solids are approximated as continuous materials: All relevant dimensions must be much larger than the atoms of which matter is composed. Historically, the concept of strain was derived from measurements of the change in length of a rod that is either stretched or compressed. When a force is applied parallel to a rod of length  $l$ , its length changes by an amount  $\Delta l$ . The length change  $\Delta l$  is observed to be proportional to the length  $l$  itself, so  $\Delta l$  depends on the size of the specimen being tested. A measure of deformation that is independent of the specimen size is obtained by taking the ratio of these two quantities to define a dimensionless *longitudinal strain* as (see Figure 3.1a):

$$\varepsilon_l = \frac{\Delta l}{l}. \quad (3.2)$$

A full description of extensional strain in a three-dimensional body requires three perpendicular longitudinal strains, one for each direction in space.

In addition to stretching or compression, a solid can also be deformed by shear, in which one side of a specimen shifts in a direction parallel to the opposite side. In the special case

of *simple shear* the top of a layer of thickness  $b$  is displaced by a horizontal distance  $\Delta x$  from the bottom, while its thickness  $b$  remains constant. In this case the *shear strain* is defined as (Figure 3.1b)

$$\epsilon_s = \frac{\Delta x}{b} \approx \theta \quad (3.3)$$

where  $\theta$  is the slope angle of the sheared material. This angle becomes exactly equal to  $\Delta x/b$  as  $\Delta x$  approaches zero. Again, because space is three-dimensional there are three independent shear strains.

Mathematically sophisticated readers may note that the six strains are not vector quantities, but form components of a  $3 \times 3$  symmetric tensor. The three perpendicular longitudinal strains are the diagonal components and the shear strains are the off-diagonal components. An important theorem states that the coordinate axes can always be rotated to a system in which the strain tensor is diagonal. In this coordinate system all strains are longitudinal, although some may be compressional while others are extensional. A general  $3 \times 3$  matrix has 9 components, not 6. The extra three (which form an antisymmetric tensor) correspond to pure rotations, which, because they do not cause distortions of the material, are wisely excluded from the definition of the strain tensor.

Finally, if all the dimensions are shrunk or expanded equally, the shape is preserved, but the volume  $V$  changes, and the resulting deformation is described by the *volume strain* (Figure 3.1c):

$$\epsilon_v = \frac{\Delta V}{V}. \quad (3.4)$$

There is only one volume strain and it depends entirely on the longitudinal strains, because it can be expressed as the sum of the three perpendicular longitudinal strains.

### 3.2.2 Stress

Stress is a measure of the forces that cause deformation. In the limit of small deformations it is linearly proportional to strain for an elastic material. Just as the strain is expressed as a ratio of the change in length divided by the length, to make it independent of the size of the test specimen, stress is expressed as the ratio between the force acting on the specimen and its cross-sectional area. Defined in this way, stress is independent of the size of the test specimen and has dimensions of force per unit area, the same as pressure. Thus, if the cross-sectional area of a rod is  $A_c$ , and a force  $F_l$  is acting to stretch or compress it, the *normal stress* in the rod is defined as:

$$\sigma_l = \frac{F_l}{A_c}. \quad (3.5)$$

Similarly to longitudinal strain, there are three normal stresses, one for each perpendicular direction of space.

Stress is defined as positive when a rod is extended. This makes stress proportional to strain times a positive number. This is a sensible procedure and is used without further comment in engineering texts, in which positive stress is tensional. However, in geologic applications stresses are nearly always compressional. Even when stretching does occur, it is often under conditions of an overall compressional background stress, so that the stress in the extended direction is simply less compressive than the other directions (in this case, the stress is often said to be extensional as opposed to tensional). For such applications it would obviously be simpler if compressional stress is taken as positive. However, such a convention complicates other simple relations in the full theory of stress and strain. Various geological authors have tried special definitions to deal with this problem, although few have gone so far as to make the constants relating stress and strain negative. Turcotte and Schubert, in their otherwise excellent book, actually switch conventions halfway through, and other authors recommend changing the sign of the strain definition. The least drastic convention, and the one followed in this book, is to define pressure as the negative of the average of the three perpendicular stresses, so that compressive (negative) stress always give rise to positive pressure. This means that a compressional stress acting on a rock mass is negative.

In close analogy to shear strains, the three *shear stresses* are defined as the ratio between a deforming force  $F_s$  and, in this case, the basal area of the sheared layer  $A_b$ :

$$\sigma_s = \frac{F_s}{A_b}. \quad (3.6)$$

Just as for strains, stresses are components of a  $3 \times 3$  tensor whose diagonal components are the normal stresses and the off-diagonal components are the shear stresses. (The three antisymmetric components of the full  $3 \times 3$  tensor are torque densities, which almost never arise in practice. We do not consider them further.) Stresses are not vectors: The forces are vectors, but because the forces are divided by an area that also has a direction in space, the stresses are components of a tensor. Stresses, thus, do not point in some direction in space. However, it is always possible to rotate the coordinate axes such that the off-diagonal shear stresses are zero in the new coordinate system, and stresses are sometimes graphically represented as triplets of arrows of different lengths pointing in perpendicular directions. But beware! Such arrows cannot be added or subtracted in the same fashion as vectors!

Finally, in the special case where the stresses are equal in three perpendicular spatial directions, the negative of the force per unit area (all directions are equivalent in this case) is defined as the pressure:

$$P = -\sigma_{\text{vol}} = -\frac{F}{A}. \quad (3.7)$$

Because stresses, and stress differences in particular, play a major role in determining the ability of a solid to resist deformation, it is often convenient to single out the three perpendicular normal stresses in the special coordinate system in which the shear stresses

vanish. These special stresses are called *principal stresses* and are frequently denoted  $\sigma_1$ ,  $\sigma_2$ , and  $\sigma_3$  for the maximum (most tensional), intermediate, and minimum (most compressive) normal stress directions – but be careful of stress conventions here: in geologic applications the maximum stress is often taken as the most compressive. So long as this is understood, it causes little difficulty. In the case of hydrostatic stress (pressure) these principal stresses are all equal. When there are three unequal deviatoric stresses the definition of pressure in Equation (3.7) is generalized so that  $p$  is equal to the negative average of the three principal stresses. This quantity plays a special role in the tensor description of stress because it is a rotational invariant, the (negative) trace of the stress tensor, divided by 3.

Because of the qualitatively different dependence of strength on pressure and shear, the stress is often separated into a component that depends only on differential stresses, called the *deviatoric stress* (often written as  $\sigma'$  – thereby forming a test of the readers' attentiveness) plus the (negative) pressure. The principal stresses are then written as  $\sigma_1' - p$ ,  $\sigma_2' - p$  and  $\sigma_3' - p$ , whereas the shear stresses are the same as before.

The ultimate strength of many materials is often found to depend on the magnitude of the difference between the maximum and minimum principal stresses,  $|\sigma_1 - \sigma_3|$ , without any dependence on the intermediate principal stress. A somewhat more complicated measure of the total distortional stress that does take the intermediate principal stress into account is called the *second stress invariant*  $\Sigma_2$  (pressure is the *first invariant*):

$$\Sigma_2 = \sqrt{\frac{1}{6} \left[ (\sigma_1 - \sigma_3)^2 + (\sigma_1 - \sigma_2)^2 + (\sigma_2 - \sigma_3)^2 \right]}. \quad (3.8)$$

The factor of 1/6 under the square root is a conventional part of the definition. There is also a *third invariant*, whose role in failure mechanics is more complex, and is not considered further in this text. These quantities are called invariants because their magnitude does not depend on the orientation of the coordinate system. Once their values are established in one coordinate system, they are the same in all.

It may seem surprising that there is no shear stress term in either of these formulas: after all, it is common experience that solids break more readily in shear than under compression. However, shear actually *is* incorporated, although this may not be apparent. The reason is that shear is one of those off-diagonal components that are intentionally eliminated by the coordinate rotation that brings the stress tensor to its diagonal form. It can be shown that a state of pure shear stress  $\sigma_s$  is equivalent to one in which the coordinate axes are rotated 45° and the principal stresses are  $\sigma_1 = -\sigma_3 = \sigma_s$ .

### 3.2.3 Stress and strain combined: Hooke's law

English scientist (and Newton's arch-rival) Robert Hooke (1635–1703) recorded some of the first observations of the relation between stress and strain in 1665. Working mainly with springs (Hooke was really interested in clocks) that produce visible deformations under

relatively small loads, Hooke hypothesized a linear relation between longitudinal stress and strain, now known as *Hooke's law*:

$$\sigma_l = E \varepsilon_l \quad (3.9)$$

where the proportionality constant  $E$  has dimensions of pressure and is generally known as Young's modulus, after a much later researcher who studied the extension of elastic rods. Although it was once believed that a single elastic constant is sufficient to describe the stress–strain relation for a given material, it was finally demonstrated in the early 1800s that at least two constants are necessary to characterize an isotropic solid (in fact, for a single crystal, up to 21 elastic constants may be necessary, but here we consider only the minimum required). The second constant is often taken to be the shear modulus  $\mu$  that relates shear stress to shear strain:

$$\sigma_s = 2 \mu \varepsilon_s. \quad (3.10)$$

The factor of 2 is a conventional part of the definition that derives from the way shear strain is defined. Because there are two elastic constants they can be, and often are, combined in various ways. For example, pressure and volume strain are related by a constant  $K$  usually known as the bulk modulus:

$$p = -K \varepsilon_v \quad (3.11)$$

(note the minus sign because of the way pressure is defined). Because there are only two independent stress–strain constants, one of these three must obviously be a function of the others: It can be shown that  $E = 9K\mu/(3K + \mu)$ .

Another useful combination is called Poisson's ratio  $\nu$ . In Figure 3.1a the extended rod is illustrated as having contracted in the direction perpendicular to its extension. This is a real, observed effect (indeed, the case of pure extension, without lateral contraction, is very difficult to realize in practice as it requires tensional loads perpendicular to the extension axis to maintain a constant cross section). The dimensionless Poisson's ratio is defined as the ratio between the amount of lateral contraction and the longitudinal extension of a laterally unconstrained rod. The deformation illustrated in Figure 3.1a actually involves both a volume change and shear (change of shape), so that the Young's modulus contains contributions from both the bulk modulus and shear modulus. In terms of Poisson's ratio,  $\nu$ , the Young's modulus is  $E = 2(1 + \nu)\mu$ .

Relations between stress and strain are generally known as *constitutive relations*. Hooke's law was simply the first of what is now understood to be a large class of possible relationships between deformation (strain) and applied force (stress). Such relations may also involve time: We will shortly meet the concept of viscosity (invented by Newton) that relates the strain *rate* (the derivative of strain with respect to time) to applied stress. In modern times the study of the relation between deformation and stress has reached a high degree of sophistication. This field is now known under the name of *rheology*. Because the materials that make up planets are complex, the rheologic properties of materials as diverse as rock, air, ice, and lava are crucial for an understanding of how the surfaces of planets and moons formed and continue to evolve.

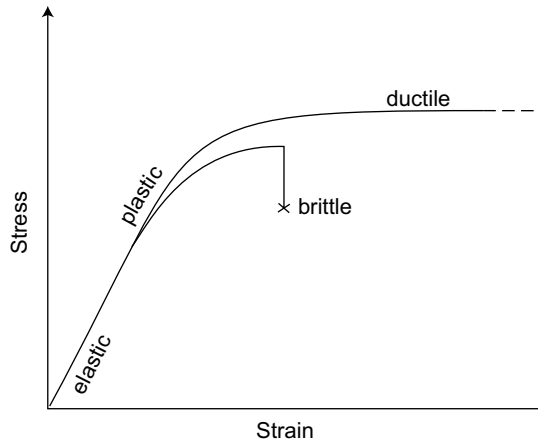


Figure 3.2 In a real solid, stress is linearly proportional to strain only for small stresses and strains (typically only up to a strain of about 0.001). Beyond this limit the relationship becomes non-linear. In this regime the flow deformation may be reversible (non-linear elasticity) or non-reversible (plastic). At even larger strains the material may fracture, losing its strength suddenly in a brittle fracture, or continue to deform to large strains in ductile flow.

The mathematically convenient linear relation between stress and strain does not hold in all, or even in most, real situations: Although stress and strain are always proportional for sufficiently small deformations, when the deformation becomes large enough (and *large* may be a strain of only 0.001 – not even visible to the human eye!) the relation becomes non-linear and catastrophic failure of various kinds may occur (Figure 3.2). Nevertheless, the combination of simple constitutive laws, such as that of Robert Hooke, and the requirement that both internal and external forces are in balance (often known under the name *stress equilibrium*) has been immensely fruitful in explaining the ability of planets to support topographic loads.

### 3.2.4 Stress, strain, and time: viscosity

Just as ideal elasticity is a useful limit describing the deformation of materials at small strains, so too is the concept of ideal viscosity. Isaac Newton first recognized viscosity on the basis of his extensive experimental studies, and proposed an ideal generalization of his experiments (in fact, Newton proposed this property mainly to undermine his rival Descartes' vortex theory of planetary motion). Ideal elasticity relates shear stress  $\sigma_s$  and shear strain  $\epsilon_s$  by a linear equation. Similarly, ideal (or *Newtonian*) viscosity relates the shear stress and shear strain *rate*  $\dot{\epsilon}_s$  through a single constant  $\eta$ , the *viscosity*:

$$\sigma_s = 2\eta\dot{\epsilon}_s. \quad (3.12)$$

Viscosity has dimensions of stress  $\times$  time, or Pa-s in SI units. The rules for viscous flow are somewhat more complicated than those of elasticity because the volume strain  $\epsilon_v$

cannot be a function of time: If it were, the volume of a viscous substance under pressure would gradually decrease to zero! Discussions of viscous flow must, therefore, pay careful attention to the difference between volume strain and shear strain. In most ideal models the volume strain is set equal to zero; this is called the incompressible limit. A more realistic, but mathematically more complex, approximation is to treat the volume strain as elastic and the shear strain as viscous.

### 3.3 Linking stress and strain: Jeffreys' theorem

#### 3.3.1 Elastic deformation and topographic support

The earliest and simplest models of topographic support are derived from applications of the classic theory of elasticity. This theory combines the full tensor definitions of stress and strain with a linear Hooke-type relation between stress and strain (with just two elastic constants, the minimum number) and the stress equilibrium equations to derive a closed mathematical system. Within the context of this theory, one can show that, starting from an unstressed initial solid, the stress and strain throughout the solid are uniquely determined by the forces and displacements acting on its surface. Thus, if we approximate a planet, or some well-defined portion of it, as an elastic solid, and treat the weight of topography as a load acting on its surface, the stress differences induced by the topography can be accurately computed throughout its interior.

Of course, this is an unrealistically rosy picture of what is actually possible: The troubles come from the detailed conditions under which elastic theory is valid. Harold Jeffreys, to whom we owe many of the results that follow, was painfully aware of the limitations of the elastic model, and he devoted much effort to understanding both its successes and its failures. The first difficulty is the obvious limitation of elastic behavior to small deformations. Once failure or flow occurs, elastic theory becomes invalid. In principle this can be addressed by numerical methods and is thus inconvenient but not insurmountable. The second, more insidious difficulty stems from the condition of an *unstressed initial solid*. All planetary surfaces with which we are familiar exhibit a long history of change, of repeated events that certainly exceeded the limits of linear elasticity. So to what extent can the near-surface material be considered *initially unstressed*?

All planetary materials have mass and all are subject to gravity, so at a minimum, the rocks beneath the surface must develop sufficient stresses to support their own weight. However, even a liquid, without resistance to deformation (but still resisting volume change!) can support its own weight. It does this by compressing slightly and thus balancing the gravitational force of the overlying material against the much stronger quantum mechanical forces that resist the close approach of atoms (gravity eventually wins this struggle in the stellar collapse to a black hole, but this is far outside the range of planetary processes). The stresses are hydrostatic in this case, and the pressure  $p$  a distance  $h$  below the surface of a body with uniform density  $\rho$  and surface gravitational acceleration  $g$  is given by:

$$p = \rho gh. \quad (3.13)$$

Although such *lithostatic* pressures may be very large compared to the stress differences needed to cause rock failure, the large value of the bulk modulus  $K$  for most substances ensures that the associated volume strain is small. In this case, we can simply add the lithostatic stress and strain of the subsurface rock to that caused by other loads. This is a consequence of the linearity of the theory of elasticity: Two solutions can always be added to give a third solution, so long as the boundary conditions of the third solution are the sums of those of its components.

If the rock beneath a planet's surface crystallizes from a deep liquid mass, or is heated to such a high temperature that all differential stresses relax after some time, then the lithostatic stress state described above can be accurately considered to be the initial state and the response to any subsequent loads can be computed as elastic additions to this basic state. Unfortunately, most planets are not so cooperative: In most cases one cannot assume that all differential stresses were erased just before the latest episode of topographic loading.

Another elastic solution useful for describing an initial state is derived from the stresses that develop in an initially unstressed and very wide elastic sheet that is suddenly subjected to the force of gravity. The elastic sheet cannot expand laterally; it can only compress vertically. In this case the principal stresses are not all equal (lithostatic), but the vertical stress  $\sigma_v$  and horizontal stresses  $\sigma_H$  differ in magnitude:

$$\begin{aligned}\sigma_v &= -\rho gh \\ \sigma_H &= -\frac{\nu}{1-\nu} \rho gh\end{aligned}\quad (3.14)$$

where  $\nu$  is Poisson's ratio, which can be no larger than 0.5. Poisson's ratio for most solid rocks is close to 0.25, although it can approach 0.0 for loosely consolidated sediments. In this solution the magnitude of the horizontal stress is smaller than the magnitude of the vertical stress. The difference between the horizontal stresses and the vertical stress increases linearly with depth and so, at some large enough depth failure must occur, but this is often so deep that the solution has great practical value.

Alert readers may wonder that this solution has any practical value at all: the idea that a mass of rock might be assembled in the absence of gravity, which is afterwards magically turned on, seems so artificial that it could not apply to any real situation. However, as demonstrated by Haxby and Turcotte (1976), this is precisely the stress state that develops in a rock mass assembled from the gradual accumulation of a stack of thin, broad and initially stress-free layers. Thus, the stresses that develop in a thick pile of lava flows, or in an accumulating sedimentary basin, are well described by this model. Compilations of vertical and horizontal stress measurements in the Earth (McGarr and Gay, 1978) show that, in many places, such as southern Africa or in sedimentary basins in North America, stresses are bounded between the lithostatic and infinite-layer results (this is not true everywhere: In Canada and much of Europe horizontal stresses are much larger than suggested by these solutions).

Although the two basic states just described are frequently useful, they are certainly not unique: Through all six editions of *The Earth*, Jeffreys invariably emphasized that, due to the generally unknown history of previous deformation, there are an infinite number of stress and strain configurations that are compatible with the presently observed topography. So why did he devote so much time and effort to obtaining elastic solutions when he did not believe that such solutions could be accurate? Jeffreys frequently cited a theorem he called *Castigliano's principle*, which asserts: "Of all states consistent with given external forces, the elastic one implies the least strain energy" (Jeffreys, Ed. 6, Appendix C). Thus, to the extent that the forces acting below a planetary surface tend toward a minimum of energy, the elastic solution delineates the favored minimum. A second reason is that, although a given elastic solution may not represent the complete stress state, it does often indicate how the stresses *change* in response to a small change in the applied loads. For example, the formation of a distant impact crater or a change in planetary spin rate or tidal stresses may cause stress changes that are accurately described by an elastic deformation. In either case, the elastic solutions are of greater significance than the limitations of the strictly conceived elastic model would suggest.

### 3.3.2 Elastic stress solutions and a limit theorem

Using the full theory of elasticity, stresses can be computed beneath various surface loads, assuming an initially hydrostatic initial state. Contour plots of the second invariant  $\Sigma_2$  for four of these configurations are shown in Figure 3.3a–d. Figures 3.3a–c apply to long loads intended to represent idealized mountain profiles, originally computed by Jeffreys. Figure 3.3d shows the stress differences underneath an axially symmetric idealized impact crater with a depth/diameter ratio of 0.3.

Although the patterns illustrated by these various solutions are diverse in detail, there are a number of similarities. Most obvious is that the maximum stress differences are not at the surface, but occur some distance below. Thus, most of the weight of a sinusoidal series of mountain ridges is not supported by the strength of the material in the mountains themselves, but by material some distance below. This is an important lesson (one ignored by the builders of the Tower of Pisa): Foundations are important! The second important lesson is that the maximum stress difference is about 1/3 of the total load itself for all four cases illustrated. These results are summarized in Table 3.1, where the depth to the maximum stress and the maximum stress differences for Figures 3.3a–d are listed.

The first lesson from these solutions, the isolation of the maximum stress region below the surface, is not strictly valid outside the domain of elastic solutions. More sophisticated analyses, using the theory of plasticity described below, show that, although first failure upon loading does, indeed, occur where the elastic solution predicts the maximum stress differences, once this failure has occurred the failure zone may work its way toward the surface, especially if the load has sharp edges, as for a cliff or steep surface slope. The final, visible failure may, thus, involve a surface landslide localized at one of these sharp edges. However, the region over which the strength of the material is

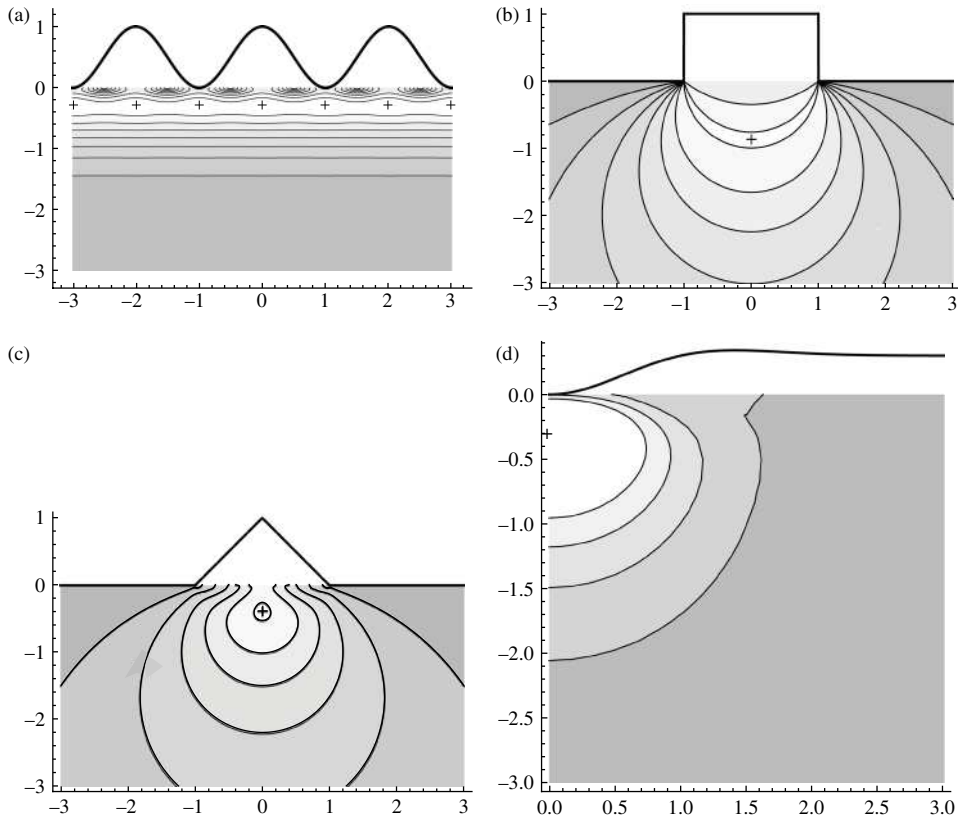


Figure 3.3 Stresses below various loads placed on an originally unstressed elastic half space. Contours are of the second invariant  $\Sigma_2$  and are drawn at intervals of 0.05, 0.1, 0.15, 0.2, 0.25, 0.3, 0.35, and 0.4 of the maximum load. These plots were constructed by summing the Fourier components of the Airy stress function that satisfies the load boundary conditions. (a) Shows the differential stress magnitudes beneath a series of very long mountains with sinusoidal hills and valleys. (b) Stresses beneath a vertical-sided strip mountain. (c) Stresses beneath a long mountain with a triangular profile and (d) Stresses beneath a circular impact crater with depth/diameter ratio 0.3. Plots are not vertically exaggerated; horizontal dimensions are in units of the load width. The + sign marks the position of the stress maximum in each plot.

exceeded is far broader than such a surface manifestation and is well delineated by the elastic solution.

The second lesson from the elastic analysis is more enduring. Generations of structural engineers have devoted their ingenuity to ways of extending their ability to analyze the maximum stresses that develop in any given structure. The results of this effort (and the subject of a huge literature of its own) are the so-called *limit theorems*. Although theorems of this type do not give the user the detailed distribution of stresses in some complex structure (this must be done on a case-by-case basis using a full knowledge of the structure and its history of loading), they do give some overall constraints on how

Table 3.1 Elastic stress differences, Poisson's ratio  $\nu = 0.25$ 

Load shape	Maximum stress difference $\Sigma_z/\rho gh$	Depth of maximum below surface
Sinusoidal strip, wavelength $\lambda$	0.384	0.289 $\lambda$
Rectangular strip, width $w$	0.352	0.865 $w$
Triangular strip, basal width $w$	0.305	0.388 $w$
Axisymmetric crater, depth/diameter=0.3, diameter $D$	0.359	0.305 $D$

strong materials must be to support some given load, independent of structure and history of construction.

As summarized by Jeffreys, structural limit theorems assure us that to support a surface load of order  $\rho gh$ , *somewhere* in the body stresses between  $1/2$  and  $1/3$  of this load must be sustained. Furthermore, this stress is generally supported at a depth comparable to the load width (exceptions to this depth rule, such as loads supported by strong, thin plates, usually imply stresses greatly in excess of the minimum).

This fundamental theorem is so important (and so often overlooked in the planetary literature!) that I set it out by itself for emphasis:

**Jeffreys' Theorem: The *minimum* stress difference required to support a surface load of  $\rho gh$  is ( $1/2$  to  $1/3$ )  $\rho gh$ . This stress is usually sustained over a region comparable in dimensions to the load.**

Of course, this theorem does not prevent much larger stresses from developing in specific situations, but a given topographic load cannot be supported by any smaller stress difference. The value of this theorem is that it can be linked to specific strength models to obtain quick estimates of the maximum topographic variation to be expected on any given Solar System body, even when the specifics of interior structure and history are unknown. An example of this procedure is given in the next section.

### 3.3.3 A model of planetary topography

Consider a generic planetary body (Figure 3.4) of mass  $M$ , average radius  $\bar{R}$  and average density  $\bar{\rho}$ . The surface acceleration of gravity  $g$  is:

$$g = -\frac{GM}{\bar{R}^2} = -\frac{4}{3}\pi G \bar{\rho} \bar{R} \quad (3.15)$$

where  $G$  is Newton's gravitational constant.

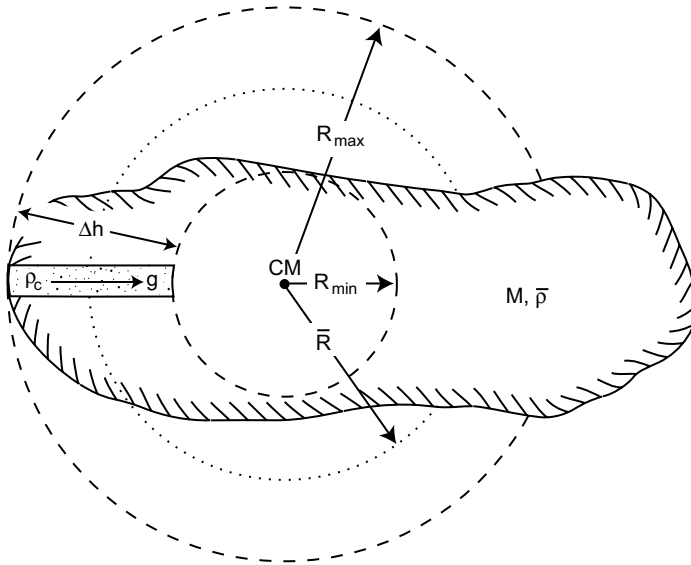


Figure 3.4 A simple model of the gravitational forces in an irregular self-gravitating body such as an asteroid. The average radius is  $\bar{R}$  and the maximum and minimum radii for points on the surface are  $R_{\max}$  and  $R_{\min}$  from the center of mass CM. The mean density of the object is  $\bar{\rho}$ .

This relation is exact for a spherical body, and approximate for any other shape. If the surface has topography of order  $\Delta h$ , and its material is of density  $\rho_c$ , the surface load imposed by this topographic variation is about  $\Delta\sigma = \rho_c g \Delta h$ . Applying Jeffreys' theorem, a minimum stress of magnitude  $Y$  must be present somewhere in the body's interior:

$$Y \approx \frac{1}{2} |\Delta\sigma| = \frac{2}{3} \pi G \bar{\rho} \rho_c \bar{R} \Delta h. \quad (3.16)$$

Rearranging, we obtain an equation that relates the maximum topographic variation,  $\Delta h$ , to some measure of *strength*,  $Y$ .

$$\Delta h \approx \frac{3}{2\pi G} \frac{Y}{\rho_c \bar{\rho}} \frac{1}{\bar{R}}. \quad (3.17)$$

Applying this equation to the Earth, take  $\bar{\rho} = 5200 \text{ kg/m}^3$ ,  $\rho_c = 2700 \text{ kg/m}^3$ ,  $\bar{R} = 6340 \text{ km}$ . We find:

$$\Delta h_{\text{Earth}} (m) \approx 80.4 Y (\text{MPa}). \quad (3.18)$$

Taking  $Y \approx 100 \text{ MPa}$ , which is about the crushing strength of granite, we see that the Earth can support about 8 km of topography – not far off the 8850 m height of Mount Everest or the 11 000 m depth of the Marianas trench, when the buoyancy of submerged rock is taken into account. However, the dependence of  $\Delta h$  on  $1/\bar{R}$  means that, if  $Y$  is the

same for all the terrestrial planets, we should expect 8 km high mountains on Venus, 24 km high mountains on Mars and 50 km high mountains on the Moon. As shown in Figures 2.3b and 2.3e, this is not far off for Venus and Mars, but is more than twice the observed topographic range on the Moon in Figure 2.3d. Evidently strength is not the major factor limiting the Moon's topography: History must play a role, too.

Applying this model for topography to the smaller bodies of the Solar System, such as Phobos, this rock strength limitation leads to ridiculous conclusions about the topographic ranges on these bodies (see Problem 3.1 at the end of the chapter). One might be tempted simply to give up and look for factors other than strength that limit topography. However, as we shall see in the next section, a better appreciation of the concept of strength lets us go considerably farther down the strength limitation path. In particular, we need to appreciate the laws that govern the strength of broken rock.

### 3.4 The nature of strength

#### 3.4.1 Rheology: elastic, viscous, plastic, and more

Rheology is the study of the response of materials to applied stress. Although stemming from roots in prehistory, E. C. Bingham (of whom we will learn much more in Chapter 5) first established it as a scientific discipline in the 1930s. It is not a simple science: Real materials are complex and so is their detailed description. However, much of this complex behavior can be understood in terms of the properties of a number of simple *ideal materials*, which are then compounded to approximate real substances. We have already described ideal elastic and viscous substances. A third ideal behavior is implicit in the idea of *strength*: An ideal *plastic* substance is one which does not undergo any strain at all until the strength reaches some limiting value, after which the strain increases to any extent consistent with other constraints on the material. Of course, no real material behaves in this way, but many materials do not undergo any very large strains until some limiting stress is reached, after which strain increases rapidly. A slightly more realistic model is to compound elastic behavior with plastic yielding to arrive at an elastic-plastic substance that responds to applied stress as an ideal elastic material until the stress exceeds some limit, after which its strain is limited only by system constraints. Then we could add materials whose elastic strain depends on a non-linear function of stress. We can add time dependence by coupling elastic and viscous behavior. And so on.

This section explores some examples of such compound behavior relevant to understanding planetary topography and its long-term evolution. The first topic we examine is the ultimate limits to topographic heights, after which we will look at more realistic limits.

#### 3.4.2 Long-term strength

*The ultimate strength of atomic matter.* A full understanding of the strength of matter was achieved only in the mid-twentieth century. Despite the triumphs of quantum mechanics in explaining the bulk properties of matter in the early twentieth century, an explanation of

strength came much later. The earliest modern attempt to compute the strength of materials from basic principles was a mitigated disaster: Yakov Frenkel (1894–1952), in 1926 (Frenkel, 1926), constructed a simple model of shear resistance (see Box 3.2 for his derivation) that relates the ultimate strength,  $Y_{\text{ultimate}}$ , of a material to its shear modulus  $\mu$ :

$$Y_{\text{ultimate}} = \mu/2\pi. \quad (3.19)$$

### Box 3.2 The ultimate strength of solids

The first estimate of the theoretical upper limit to the strength of a solid was formulated by Yakov (a.k.a. Jacov or James) Frenkel (1926). Frenkel started from the fact that atoms in a crystal lattice are uniformly spaced at the interatomic distance  $a$ . When a solid is subjected to shear strain, each plane of atoms parallel to the direction of the strain shifts a small distance  $u$  with respect to the plane immediately above or below. The net shear strain is thus given by  $\epsilon_s = u/a$ , and is numerically the same at both the atomic and macroscopic scales (see Figure B3.2.1). The force resisting this deformation increases as one plane of atoms shifts over the adjacent plane, because the length of the bonds between each atom and its neighbor increases. However, when the deformation becomes so large that the atoms of adjacent planes are midway between lattice sites (that is, at a strain  $\epsilon_s$  equal to  $1/2$ ), the attraction to the next atom in the adjacent plane equals the attraction from the shifting atom's previous neighbor and the resistance to deformation drops to zero. Further deformation brings each atom into closer proximity to its new neighbor. New bonds form: The atomic plane snaps into a new position, jumping forward by one atomic step.

The force between adjacent atomic planes of a strained crystal is thus periodic, with a repeat distance equal to the interatomic spacing. Frenkel assumed that this periodic function would be the simplest that he could think of: A sine function. He set the force resisting deformation equal to a constant times  $\sin(2\pi u/a)$ . Because the maximum value of the sine function is 1 (when  $u = a/4$ ), the constant equals the ultimate strength of the crystal,  $Y_{\text{Frenkel}}$ . Thus, he supposed that the shear stress is given by:

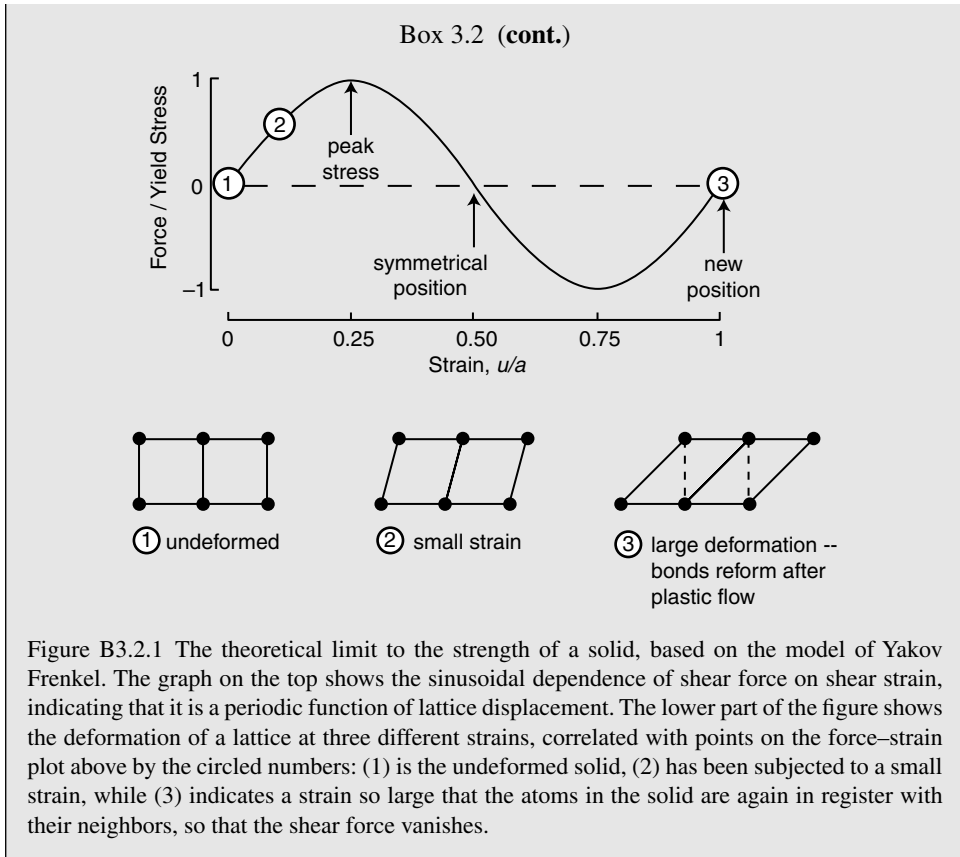
$$\sigma_s = Y_{\text{Frenkel}} \sin\left(\frac{2\pi u}{a}\right) = Y_{\text{Frenkel}} \sin(2\pi\epsilon_s). \quad (\text{B3.2.1})$$

To determine the constant, he noted that very small deformations are elastic, and in this limit  $\sigma_s = \mu\epsilon_s$ . Expanding the sine function for very small arguments yields Frenkel's relation for the ultimate strength of a solid in terms of the shear modulus  $\mu$ ,

$$Y_{\text{Frenkel}} = \frac{\mu}{2\pi}. \quad (\text{B3.2.2})$$

Although defect-free solids such as fine whiskers and carbon microtubules can approach this limit, Table 3.2 shows that Frenkel's limit greatly overestimates the strength of real materials, even for rocks at high confining pressures.

Accurate computation of the actual strength of materials is not yet possible, so that measurement and empirical estimates are still necessary to determine the strength of a real substance under conditions of interest to planetary science.



The shear modulus has been measured for a large variety of materials. It is a bulk property that can now be computed from first principles for many single crystals. Although Frenkel's formula is elegantly simple, it is also grossly inadequate: As shown in Table 3.2, the actual measured strength of most materials is a factor of 100 or more smaller than the Frenkel limit. Nevertheless, the Frenkel limit is not wholly wrong or useless: The strength of a few materials, such as carefully prepared single crystals or fine carbon fibers, does approach this limit. However, the Frenkel limit clearly does not capture the factors controlling the strength of the materials we are likely to meet in planetary interiors.

The principal shortcoming of Frenkel's strength estimate is its neglect of *defects*. Rocks are composed of crystals of individual minerals. While the crystals themselves might be strong, they are bonded through weaker surface interactions. Most igneous rocks, such as granite or basalt, have cooled through a large range of temperatures and, because of the different thermal expansion coefficients of their constituent minerals, tiny grain-boundary cracks develop in abundance. Sedimentary and metamorphic rocks also contain vast numbers of microscopic cracks and weak bonds between individual grains. All rocks contain

Table 3.2 *Theoretical vs. observed material strength*

Solid material	$Y_{\text{ultimate}}$ $= \mu/2\pi$ (GPa) <sup>a</sup>	$Y_{\text{observed}}$ At $p = 1$ and $5$ (GPa) <sup>b</sup>
Iron, Fe	13.0	0.11–1.0
Aluminum, Al	4.14	0.10–0.30
Corundum, Al <sub>2</sub> O <sub>3</sub>	25.9	0.26–0.92
Periclase, MgO	20.9	0.14–1.07
Quartz (Opal), SiO <sub>2</sub>	7.08	0.35–1.8
Forsterite, Mg <sub>2</sub> SiO <sub>4</sub>	12.9	1.13 ( $p = 0.5$ GPa) <sup>c</sup>
Calcite, CaCO <sub>3</sub>	5.09	0.27–0.84
Halite, NaCl	2.34	0.09–0.29
Ice, H <sub>2</sub> O	0.54	0.20–1.0 <sup>d</sup>

<sup>a</sup> Elastic moduli from Bass (1995).

<sup>b</sup> At 23°C from Handin (1966) Table 11–9, except as noted.

<sup>c</sup> At 24°C Handin (1966), Table 11–3, Dun Mtn., NZ, peridotite.

<sup>d</sup> At 77–115 K; extrapolated from Beeman *et al.* (1988).

macroscopic cracks in the form of joints. In addition to cracks between mineral grains, the minerals themselves inevitably contain arrays of a peculiar sort of strength-related line defect called *dislocations*. First described in the 1950s by engineers studying the creep elongation of turbine blades in high-temperature jet engines, dislocations flow under stresses far below the Frenkel limit. It is only by studying the properties and interactions of entities such as cracks and dislocations that progress has been made in understanding the practical limitations on the strength of materials.

Although the strength of materials is a large field of endeavor in itself, one too vast to cover in this book (references for this literature are provided at the end of this chapter), the basic take-away lesson is that defects rule the macroscopic strength properties of materials. One cannot expect planetary materials to be stronger than a small fraction of the Frenkel limit. And, in spite of a half-century of progress in understanding the fundamental basis of strength, there are so many complex contributing factors that the strength of a particular material under given conditions of pressure, temperature, and chemical environment is still best determined by experiment.

Traditional material science focuses on the strength properties of metals. Only recently have the much more complex problems presented by the strength of ceramics and geologic materials, such as rocks, become amenable to rational explanation. Naturally, experimenters did not wait for theoreticians to make up models of the strength of rock, so that much of our present understanding is based upon empirical observations.

*Built upon sand: The strength of broken rock.* Most experts on asteroids now believe that all but the very smallest asteroids (bigger than a few tens of meters in diameter) are better described as fragmented *rubble piles* than as solid chunks of rock. Unlike solid rock, rubble

piles have no tensile strength. Their entire ability to resist changes in shape depends on the frictional forces acting across the rock–rock contacts between their components.

Coulomb in 1785 first formulated the laws governing the mechanical behavior of a mass of broken rock (or a pile of sand). Because the frictional resistance at a rock–rock contact is proportional to the force pushing the rocks together, the strength of a mass of broken rock is proportional to the pressure. This fact was first clearly stated by Leonardo da Vinci (1452–1519) in the fifteenth century, but not published by him. Guillaume Amontons (1663–1705) in 1699 resurrected this relation from da Vinci’s codices. This behavior is in stark contrast to the strength of ductile metals, such as aluminum or steel, which is nearly independent of pressure. Many experimental studies of the strength of sand or soil show that the mass begins to yield when the applied shear stress  $\sigma_s$  reaches a constant fraction of the overburden pressure  $p$ :

$$|\sigma_s| = f_f p = \tan \phi_f p \quad (3.20)$$

where  $f_f$  is the *coefficient of friction* and  $\phi_f$  is the related *angle of internal friction*. This angle is also closely related to  $\phi_r$ , the angle of repose, which is the maximum steepness of a slope composed of this material (See Section 8.2.1 and Table 8.1 for more on internal friction). This coefficient is typically about 0.6 for most geologic materials (including water ice well below its freezing point), making  $\phi_f$  about 30°.

Applying this formula to a model of small-body topographic support, the most obvious evidence of topography on small bodies is the difference between their longest and shortest dimensions,  $R_{\max} - R_{\min}$  (refer back to Figure 3.4) This *out of roundness* corresponds to a load of breadth comparable to the mean radius of the body itself,  $\bar{R}$ . The stress supporting this load is, thus, localized deep within the body. The average pressure in the center of a homogeneous body ( $\rho_c = \bar{\rho}$ ) is  $p_{\text{ctr}} = \frac{1}{2} \bar{\rho} g \bar{R}$ , so that the *strength*,  $Y$ , or resistance to yield, is  $Y \approx f_f p_{\text{ctr}}$ . Inserting this into the equation for  $\Delta h$ , we find that a small-body model of strength implies:

$$\Delta h_{\text{smallbody}} \approx f_f \bar{R}. \quad (3.21)$$

Another way of deriving the same result is to note that a constant coefficient of friction implies a constant angle of repose, which is nearly equal to the angle of internal friction. Imagine a hypothetical, maximally out-of-round asteroid constructed in such a way that every slope on its surface is at the angle of repose in its local gravitational field (such a shape has now been constructed by Minton, 2008). Although the precise shape is complex, it is clear that, in traversing the surface of the asteroid from equator to pole, a distance of  $(\pi/2)\bar{R}$ , up (or down) a constant slope of angle  $\phi_r$ , an elevation change of the order of  $(\pi/2)\bar{R} \tan \phi_r$  must take place. This yields essentially the same  $\Delta h_{\text{smallbody}}$  as above.

This small-body topography model predicts that the maximum fractional deviation from sphericity,  $(R_{\max} - R_{\min})/\bar{R}$ , is actually *independent* of size. This is in strong contrast to the constant-strength model derived for the Earth, which suggests that, as a body becomes larger, its shape becomes relatively closer to a spheroid because  $(R_{\max} - R_{\min})/\bar{R} \propto 1/\bar{R}^2$ , so that the ratio decreases as  $\bar{R}$  increases.

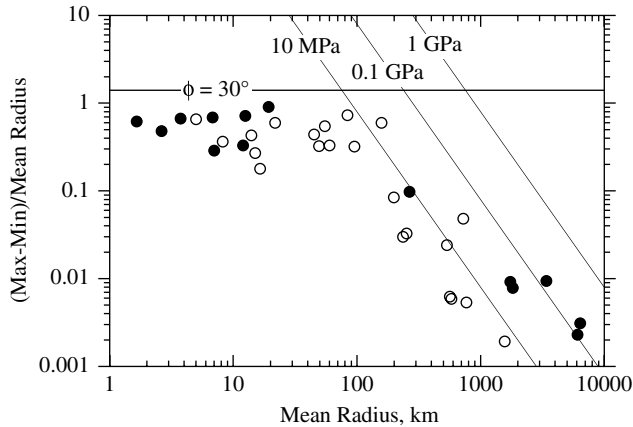


Figure 3.5 The ratio of the maximum elevation difference to the radius for various Solar System bodies as a function of diameter. Up to a diameter of about 200 km, this ratio is nearly constant, as expected for rubble piles supported only by frictional strength. Above this diameter the ratio falls off, consistent with an ultimate planetary crustal strength of about 0.1 GPa. The solid dots are silicate bodies and the open circles are icy. The data suggests that icy bodies are weaker than silicate objects although they have similar friction coefficients.

How do these model predictions fare against reality? Figure 3.5 plots the maximum fractional deviation from sphericity against mean radius for a variety of Solar System objects. It is clear that the topography of the smaller bodies does, indeed, follow a law that suggests the dominance of frictional strength. There is no obvious tendency for the fractional topographic deviation to decrease with increasing size. However, at a radius of about 200 km the frictional relationship breaks off and the maximum topographic deviations of the larger planets and moons decrease sharply with increasing diameter, following an approximate  $1/\bar{R}^2$  dependence on the log–log plot. For these large objects greater size does imply greater smoothness. The trend of the curve for larger planetary objects suggests that the ultimate strength of planetary crusts is about 0.1 GPa.

The constancy of the maximum fractional deviation for small objects is a direct consequence of the ability of pressure to increase the strength of broken rock materials. Obviously, however, this frictional increase in strength has its limits. This fact is also clear from laboratory measurements of rock strength: As shown in Figure 3.6, the frictional regime holds up to some maximum stress, generally a few GPa, when the intrinsic strength of the rock is reached and yielding occurs in spite of increasing overburden pressures. As in the large–planet topography model, it seems that the ultimate limit to topography lies in the ultimate ability of matter to resist deformation. It is thus worth inquiring just what determines this resistance.

*David Griggs and the strength of rocks.* The most obvious feature of the rocks outcropping on the surface of the Earth is that they are pervaded by fractures at all scales. How these fractures actually form, however, is much less obvious. It took many years before experimenters could reproduce the pressures and temperatures existing in the Earth's

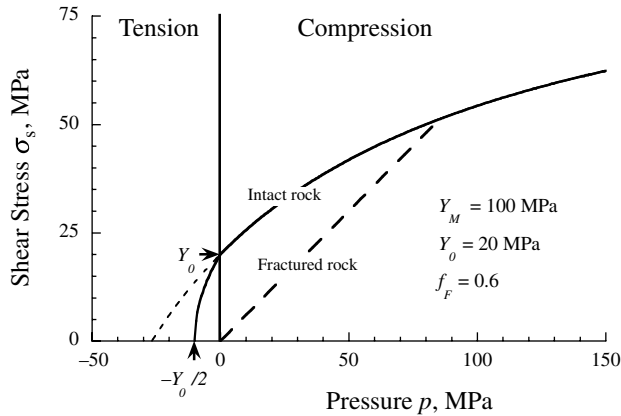


Figure 3.6 Yield stress of a *typical* intact rock specimen (heavy line) described by the Lundborg strength envelope, Equation (3.23). Note the substantial tensional strength (equal to  $Y_0/2$  by the Brace construction, which is, nevertheless, weaker than the extrapolation of the Lundborg strength envelope, shown by the dotted line, would suggest) indicated on the negative pressure axis. Shown also as a heavy dashed line is the yield curve for a fractured rock specimen for which the shear resistance is entirely due to friction.

interior and come to an understanding of how rocks break. Indeed, this is still an active area of research in the earth sciences. David Griggs (1911–1974) was one of the first people to systematically investigate rock fracturing under high pressures and temperatures. Griggs' interest in geologic processes began as a boy, when he accompanied his father, geologist Robert Griggs, on a National Geographic expedition to study the deposits of the famous 1912 eruption of Mount Katmai in Alaska (Griggs, 1922). From his experience in the field, David decided to study how rocks break deep within the Earth. He sought out Percy Bridgeman at Harvard University and signed on as his graduate student in 1933. Bridgeman's laboratory was one of the few places in the world where pressures approaching those deep in the Earth's crust could be attained.

Griggs eventually perfected an apparatus widely known as a *Griggs' rig* that could both compress and heat a small rock sample, typically a cylinder a few centimeters in length and diameter, while subjecting it to controlled differential stresses. Continuing his work after World War II at UCLA, and accompanied by a growing number of similarly motivated experimenters, he showed that, unlike metals, the fracture strength of rock is a strong function of both pressure and temperature.

It has long been known that metals and alloys, such as iron or steel, fail at similar stresses under both compression and tension. Ideal plasticity is a useful approximation to metal failure, in which half the stress *difference* at failure (equivalent to the shear stress through a coordinate rotation) is assumed to be a constant  $Y$ , the *yield stress*:

$$|\sigma_s| = \frac{|\sigma_1 - \sigma_3|}{2} = Y. \quad (3.22)$$

Table 3.3 *Lundborg strength parameters for representative rocks*

Rock	Friction coefficient, $f_f$	Cohesion, $Y_0$ (MPa)	Von Mises plastic limit, $Y_M$ , (MPa)
Granite I	2.0	60	970
Granite II	2.5	50	1170
Quartzite	2.0	60	610
Gray slate	1.8	30	570
Black slate	1.0	60	480
Limestone I	1.2	30	870
Limestone II	1.0	20	1020
Sandstone	0.7	20	900

Data from Lundborg (1968).

The yield stress of metals is, to a good approximation, independent of pressure and strain, although it declines with increasing temperature. Because of its utility in engineering, the theory of failure of ideally plastic materials is highly developed, in spite of serious mathematical difficulties that stem from this very lack of dependence on strain (Hill, 1950).

Experimental studies of rock fracture show, however, that the strength of rock depends very strongly on pressure, at least up to pressures approaching 5 GPa (50 kilobars). Many analytic representations of the failure strength of rock have been proposed; among them, one that seems to fit many materials was suggested by Lundborg (1968) for unfractured rock:

$$|\sigma_s| = Y_0 + \frac{f_f p}{1 + \left( \frac{f_f p}{Y_M - Y_0} \right)} \quad (3.23)$$

where  $Y_0$  is the strength at zero pressure, often called *cohesion*, and  $Y_M$  is known as the von Mises plastic limit of the material.  $Y_M$  limits the maximum stress that can be achieved at arbitrarily high pressure. The Lundborg form of the failure law is illustrated in Figure 3.6 and some representative values of the parameters are listed in Table 3.3.

Although the Lundborg law, and others like it, gives a good description of the failure of rock over the full range of pressures from very low to very high, much more data has been collected in the low pressure regime where a linear version is generally adequate. Thus, when  $p \ll Y_M$ ,

$$|\sigma_s| = Y_0 + f_f p \quad \text{for } p \ll Y_M. \quad (3.24)$$

Table 3.4 lists representative values of  $Y_0$  and  $f_f$  for a small number of materials, ranging from a hard igneous rock (at crustal temperatures) to weak sedimentary rock.

Table 3.4 *Low-pressure failure envelope for representative rocks*

Rock	Friction coefficient, $f_f$	Cohesion, $Y_0$ (MPa)
Westerly granite @ 500°C	0.6	50
Pennant sandstone @ 25°C	0.97	35
Limestone @ 25°C	0.75–1.6	3.5–35
Siltstone @ 25°C	0.55	21
Chalk @ 25°C	0.38	0.9

Data from Handin (1966).

The sloping, low-pressure portion of the failure law illustrated in Figure 3.6 is superficially similar to that of sand. However, in this case the pressure coefficient  $f_f$  is less obviously related to friction, although it is often referred to as a coefficient of *internal friction*, presumably because it is dimensionless and relates strength linearly to overburden pressure, as does the true friction coefficient. Numerically, it is also similar to the coefficient of rock-on-rock friction, although the reader should not confuse the two:  $f_f$  is the (approximate) linear slope of the strength envelope that defines the stress conditions under which intact rock fails, whereas  $f_B$  is the (static or starting) coefficient of friction of a pre-existing planar rock fracture sliding over another. The difference between these two curves is responsible for the *brittle–ductile* transition that gives rise to discrete faults in rock, as will be discussed in more detail in Section 4.6.1.

Extensive tables of the strength envelopes of rocks under various conditions can be found in Handin (1966) and Lockner (1995). The ultimate strength limit of about 0.1 up to 1 GPa for real rocks is in fair agreement with the observed trend of topographic deviations on the larger planets illustrated in Figure 3.5. It, thus, appears that we presently have a good first-order understanding of the strength properties of planetary bodies, although many details remain to be worked out.

The presence of pre-existing fractures in most large rock masses greatly complicates analyses of the strength of rock. The actual strength of a large volume of rock generally lies somewhere between that of intact rock and that defined by the coefficient of friction (the dashed line in Figure 3.6). A constant value of the friction on a pre-existing fracture,  $f_B \approx 0.85$  (up to a mean pressure  $p$  of about 100 MPa; the slope is somewhat less at larger pressure) is often known as *Byerlee's law* after the researcher who showed that this value describes the friction of a wide variety of rock surfaces (Byerlee, 1978). In its exact form Byerlee's law states:

$$\sigma_s = \begin{cases} 0.85 \sigma_n & \sigma_n < 200 \text{ MPa} \\ 50 + 0.6 \sigma_n & \sigma_n \geq 200 \text{ MPa} \end{cases} \quad (3.25)$$

where  $\sigma_n$  is the normal stress across a fracture,  $\sigma_s$  is the shear stress and all stresses are in megapascals.

Note that the *mean pressure*,  $p$ , in Equation (3.23) is somewhat confusingly equal to the negative of either one-half of the sum of the maximum and minimum principal stresses, or (more correctly, if less frequently seen) to one-third of the sum of all three principal stresses. A similar equation is often written in which, in the location occupied by the term  $p$  in Equation (3.23), a term for the normal stress acting across the failure plane appears instead. Byerlee's law is strictly valid only for this normal stress. The disadvantage of this formulation is that the failure plane must be known before the equation can be applied. Thus, for the present goal of defining a strength envelope, a formulation in terms of stress invariants (pressure and shear stress) is preferable. The wary user of data tables is careful to make sure which definitions are in use before accepting a given *coefficient of internal friction* at face value!

The *mean pressure*,  $p$ , in the Equation (3.23) must be modified by subtracting the pore fluid pressure,  $p \rightarrow p - p_f$ , when the rock is pervaded by a fluid that itself is at some hydrostatic pressure  $p_f$ . This modification is very important when a fluid such as water or oil on Earth, or methane on Titan, is present. It was first introduced by Terzaghi (1943) for soils, and by Hubbert and Rubey (1959) for rocks. Its detailed implications are the subject of a large literature. It will be discussed further in Section 8.2.1, but suffice it to say now that high fluid-pore pressures cause substantial weakening of rock through this pressure subtraction effect.

The coefficient  $Y_0$  in Equation (3.23) is the zero-pressure strength or cohesion. Mathematically, it is the intercept of the strength envelope with the zero-pressure axis (see Figure 3.6). Physically, it represents the adhesion of crystals in the rock to one another and can range from only a few megapascals for weak sedimentary rocks to several tenths of a gigapascal for intact granite. It is strongly affected by pre-existing cracks in the rock and drops to zero in a fully fractured rock mass. An extrapolation of this line to negative values of  $p$  intercepts the pressure axis (zero shear stress) at  $p_T = -Y_0/f_f$ . This intercept corresponds to the tensile strength of the rock. The linear extrapolation yields an overestimate of the actual yield stress by a factor of two to three: More sophisticated models based on crack theory (Brace, 1960) give a different, and more accurate, analytic form for tensile stresses that is indicated by the heavy yield curve on Figure 3.6.

The slope of the failure curve decreases at large values of the average pressure, and the maximum shear stress that the rock can sustain approaches a constant  $Y_M$ , independent of pressure. This rollover occurs when the frictional stress of sliding on inter- and intracrystalline cracks approaches the intrinsic strength of the individual crystals. A full understanding of this process is still under development, but the general outlines are now in fairly good agreement with observations (Ashby and Sammis, 1990). This change in the dependence of the strength on pressure is known as the *brittle-ductile* transition, for reasons that will be discussed in more detail in the next chapter, Section 4.6.1. It occurs at, or near, the point where the failure curve for fractured rock crosses that for intact rock in Figure 3.6.

The ultimate yield stress  $Y_M$  in Equation (3.23) is, as shown in Figure 3.6, still far below the Frenkel limit because of intra-crystalline defects such as dislocations. Although independent of pressure, by definition, it does depend strongly on temperature. There is

no universal law for this temperature dependence, which must be determined empirically, but it is clear that the strength must vanish at the melting temperature,  $T_m$ . Using this hint, a widely used approximation to the temperature dependence is to multiply both  $Y_0$  and  $Y_M$  by the same factor:

$$F_T = \left( \frac{T - T_m}{T_m} \right)^2 \quad (3.26)$$

which assures that the strength falls to zero as the temperature approaches the melting point. The exponent in this relation is purely empirical, chosen to fit a large body of data on both metals and rocks.

### 3.4.3 Creep: strength cannot endure

*David Griggs and the flow of rocks.* When David Griggs began his now-classic work in 1933 he was already the veteran of many geologic field excursions and knew from personal experience that the rocks of the Earth's crust often show signs of large amounts of deformation *without* fracture. This fluid-like deformation had long been attributed to the high pressure and temperature within the inaccessible depths of the Earth, but no one understood the rates or conditions under which this flow occurred. Griggs began his lifework with a relatively simple apparatus that measured the slow deformation of rocks under an applied load as a function of time, initially working at room temperature and pressure (Figure 3.7). Although he found that most rocks deform elastically only for periods of time less than a year, he discovered a few that exhibited slow *pseudoviscous flow* or creep according to a simple law relating the strain  $\varepsilon$  and time  $t$ :

$$\varepsilon = A + B \log t + C t \quad (3.27)$$

where the constant  $A$  represents *instantaneous* elastic deformation,  $B$  a kind of decelerating creep now often called *primary* creep, and  $C$  is the rate of steady, long-term flow. Although the primary creep term is important for short-term flow processes, such as the response to fluctuating tidal stresses or the small strains that accompany planetary reorientation and spin changes, most geologic interest centers on the third, steady-state term, because it represents deformation that increases steadily with increasing time, apparently without limit. In this respect the flow of rocks resembles that of more familiar viscous liquids, such as honey, motor oil or tar.

Sixty years of subsequent research by Griggs and a large cadre of laboratory geologists who recognized the importance of this research has shown that the rate of steady-state creep is a function of stress, temperature, and pressure, as well as rock composition, grain size, presence or absence of water, trace elements, and a host of other factors. Most creep experiments can be fit by a formula of the form:

$$C = \dot{\varepsilon}_{\text{steady}} = A_c \sigma^n e^{-\frac{Q^*}{RT}} \quad (3.28)$$

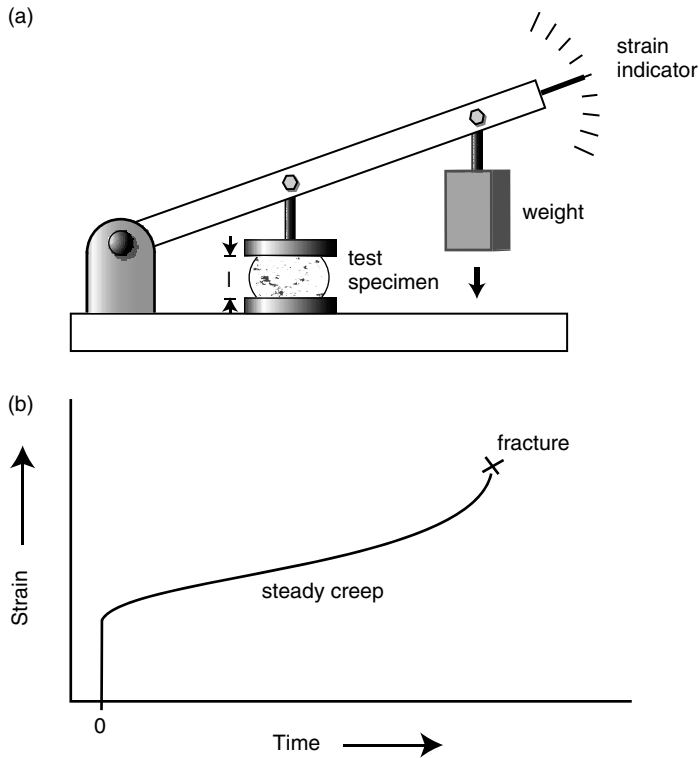


Figure 3.7 Schematic representation of a creep experiment on rock, similar to Griggs' 1933 room-temperature measurements. (a) The test specimen, of original length  $l$ , is mechanically loaded (by a weight and a lever) while its deflection is measured on a sensitive scale. (b) Schematic creep curve, showing strain as a function of time after loading. The curve shows three distinct portions after the initial elastic deflection: A period of decelerating creep, a long period of steady creep and, for lab specimens, a final acceleration just before rupture.

where  $A_c$  is a constant with dimensions  $(\text{stress})^{-n} \text{time}^{-1}$ ,  $\sigma$  is deviatoric stress,  $n$  a dimensionless constant,  $Q^*$  is *activation enthalpy* (this term incorporates most of the pressure dependence because  $Q^* = E^* + pV^*$ , where  $p$  is pressure and  $E^*$  and  $V^*$  are constants),  $R$  the gas constant, and  $T$  is absolute temperature. The dot over the strain  $\dot{\epsilon}$ , following Newton's *fluxion* notation, indicates differentiation with respect to time.

It is often convenient to express the rate of steady-state creep, Equation (3.28), in terms of an *effective* viscosity, even though it depends on the stress level. Adapting the definition of viscosity, Equation (3.12), the effective viscosity  $\eta_{\text{eff}}$  is defined as:

$$\eta_{\text{eff}} = \frac{\sigma_s}{2 \dot{\epsilon}_{\text{steady}}} = \frac{e^{\frac{Q^*}{RT}}}{2 A_c \sigma^{n-1}}. \quad (3.29)$$

This definition of viscosity generalizes Newton's original definition, which applies to the case  $n = 1$ . It has now become common to refer to the case  $n = 1$  as "Newtonian viscosity" and to use the term "viscosity" in the broader sense for any value of  $n$ , as long as it refers to a flow law in which the strain rate is a function of stress.

Unlike viscous liquids, the power  $n$  relating stress and strain rate is usually larger than 1 for creeping rocks and minerals, justifying the use of the term "pseudoviscous" for this kind of flow. Doubling the stress on materials such as ice or olivine may cause the creep rate to increase by a factor of 10, in strong contrast to ideally viscous materials in which the creep rate only doubles. It is also important to realize that creep rate depends exponentially on the temperature. Although rocks deform very slowly at low temperatures, as the temperature climbs toward the melting point the creep rate increases rapidly (by as much as a factor of 10 for each 100°C increase in temperature for many rocks). A useful approximation is that for most materials, creep rates become important over geologic time periods (millions of years, which implies  $\dot{\epsilon}_{\text{steady}} \approx 10^{-13} \text{ s}^{-1}$  or less) when the temperature reaches one-half the melting temperature,  $T \sim 1/2T_m$ . A useful simplification of the temperature dependence of the creep rate is to absorb the activation energy and melting temperature into a constant  $g$  and express the temperature as the dimensionless ratio  $T/T_m$ , the *homologous temperature*:

$$C = \dot{\epsilon}_{\text{steady}} = A_c \sigma^n e^{-g \frac{T_m}{T}}. \quad (3.30)$$

Table 3.5 gives typical values for  $A_c$ ,  $n$ ,  $Q^*$ ,  $T_m$ , and  $g$  for a few materials of geologic and planetary interest.

Extensive tables, such as that of Kirby and Kronenberg (1987a, b) and Evans and Kohlstedt (1995), have been compiled to categorize the creep of rocks, and theoretical models have been developed to explain this flow behavior in terms of diffusion and dislocation motion (e.g. Evans and Kohlstedt, 1995; Poirier, 1985). However, for the purposes of this book the principal concept to remember is that at high temperatures rocks can flow like liquids over geologic timescales.

*J. C. Maxwell and the viscosity of "elastic solids."* Observation and experiment have taught us that cool materials (that is, materials at temperatures well below their melting point) deform elastically under applied loads, while hot materials gradually flow. Elastic behavior is mostly recoverable: that is, when the load is removed the deformation reverses itself; while viscous flow is not recoverable: when the load is removed the deformation remains. The alert reader might wonder how these very different types of behavior can be reconciled at intermediate temperatures: At what point does the elastic response stop and viscous flow take over?

This important question received a definitive answer from an unlikely source. Most people who recognize the name of nineteenth-century physicist J. C. Maxwell (1831–1879) think immediately of Maxwell's equations that describe electric and magnetic fields, or perhaps of his contributions to thermodynamics and statistical mechanics. In fact, it was during his 1867 study of the viscosity of gases that Maxwell faced the puzzling dichotomy

Table 3.5 Creep properties of selected materials

Material	$A_c$ (MPa <sup>-n</sup> s)	$n$	$Q^*$ (kJ/mol)	$T_m$ (K)	$g$ $= Q/RT_m$
Olivine				2200	27
Dry	$1.2 \times 10^2$	3.0	502		
Wet	$2.0 \times 10^3$	3.0	420		
Diabase				1100	53
Dry <sup>a</sup>	5.4–347	4.7	485		
Wet <sup>b</sup>	$6 \times 10^{-2}$	3.05	276		
Quartz				1996	8.1
Dry	$1.3 \times 10^{-6}$	2.7	134		
Wet	$2.0 \times 10^{-2}$	1.8	167		
Granite (Westerly)				1320	12.7
Dry <sup>c</sup>	$2.5 \times 10^{-9}$	3.4	139		
Wet <sup>c</sup>	$2.0 \times 10^{-4}$	1.9	137		
Anorthosite	$3.2 \times 10^{-4}$	3.2	238	1400	20.5
Halite, NaCl	6.3	5.3	102	1074	11.4
Water ice, Ih, <sup>d</sup> $T > 258$ K $\sigma > 1$ MPa	$6.3 \times 10^{28}$	4	181	273	80
Solid CO <sub>2</sub> , $150 < T < 190$ <sup>e</sup>	$4.4 \times 10^3$	4.5	31	217	17
Limestone, Dry, Solenhofen ls	$2.5 \times 10^3$	4.7	298	1520	23.6

Data is from Evans and Kohlstedt (1995), except as noted:

<sup>a</sup> Mackwell *et al.* (1998)

<sup>b</sup> Caristan (1982)

<sup>c</sup> Kirby and Kronenberg (1987b)

<sup>d</sup> Durham and Stern (2001)

<sup>e</sup> Durham *et al.* (1999)

between the elastic and viscous behavior of solids (Maxwell, 1867). His insight came from what might seem like an annoying detail: The steel wire supporting the torsion pendulum he was using to measure gas viscosity exhibited viscous behavior of its own. He invented a theory of what are now known as viscoelastic materials to separate the viscosity of the pendulum wire from that of the gas.

Maxwell proceeded by postulating that the total deformation of his wire is the simple sum of the elastic plus the viscous strain,  $\epsilon_{\text{total}} = \epsilon_{\text{elastic}} + \epsilon_{\text{viscous}}$ . He supposed that each strain would develop under the influence of the same stress, obeying the equations previously stated for ideal elastic and viscous behavior. His equation, however, suffers a serious mathematical problem, because the viscous strain is not determined directly from the stress: The stress determines only the strain *rate*. It is possible to write the viscous strain as the time integral of the strain rate, but it is more straightforward to differentiate both sides of Equation (3.10) with respect to time and sum the result to obtain the fundamental equation

for a *Maxwell viscoelastic* substance,  $\dot{\epsilon}_{\text{total}} = \dot{\epsilon}_{\text{elastic}} + \dot{\epsilon}_{\text{viscous}}$ . Inserting the definitions of each term:

$$\dot{\epsilon}_{\text{total}} = \dot{\sigma}/2\mu + \sigma/2\eta. \quad (3.31)$$

This equation embodies both an elastic response for loads applied quickly and viscous flow for long sustained loads. Its full solution is complex because volume strain and shear strain must be treated differently in each term of the full tensor equation. However, it is not necessary to actually solve this equation to attain an insight of major importance. Simple dimensional analysis shows that the ratio of the viscosity  $\eta$  to the elastic shear modulus  $\mu$  has the dimensions of time. This ratio is known as the *Maxwell time*  $\tau_M$  and it plays a fundamental role in the transition from elastic to viscous behavior. Its definition is:

$$\tau_M \equiv \frac{\eta}{\mu}. \quad (3.32)$$

If a load is applied instantaneously to a Maxwell viscoelastic material, then held constant, the Maxwell time is equal to the length of time that passes before the accumulated viscous strain equals the instantaneous elastic strain. Thus, for times shorter than the Maxwell time, the material response is dominated by the elastic deformation. For times longer than the Maxwell time, the response is essentially viscous. Maxwell supposed that even water must act as an elastic material on a short enough timescale, but he computed this time as about  $10^{-13}$  s – unobservably small in the late 1800s. However, he did later succeed in observing both elastic and viscous behavior in Canada balsam (pine tree sap).

Although Equation (3.32) was derived from the equations for ideal elastic and viscous substances, a generalization of the idea of Maxwell time can be applied even to pseudoviscous materials that do not obey the equation of ideal viscosity: The generalized Maxwell time is the length of time over which creep must act for the total creep strain to equal the elastic strain. In the form of an equation:

$$\tau_M = \frac{(\text{elastic strain})}{(\text{creep strain rate})} = \frac{\epsilon_{\text{elastic}}}{\dot{\epsilon}_{\text{creep}}}. \quad (3.33)$$

The Maxwell time is often surprisingly short. This is because the elastic strain in most geologic materials is invisibly small – typically only about 0.0001, even for stresses near fracture. For this reason Australian geologist S. Warren Carey invented a term, which he called *rheidity* (Carey, 1953), and for which he proposed a timescale of exactly 1000  $\tau_M$ . Although this rheidity concept adds nothing fundamental to the idea of Maxwell time, it does give an estimate of the time necessary for viscous or pseudoviscous flow to become *visible* to the human eye.

Most children are familiar with the high-polymer material known as *Silly Putty*<sup>TM</sup>, which behaves as a brittle elastic material on a short timescale – it can be fractured by a hammer blow – but flows like a liquid when left undisturbed for a long period. It is less widely appreciated that *all* materials behave this way, if only the timescale is chosen appropriately. Water ice is another example: ice cubes in common experience are brittle elastic materials,

Table 3.6 Maxwell time and rheidity time for various materials

Material	Shear modulus, $\mu$ (GPa)	Viscosity, $\eta$ (Pa-s)	Maxwell time, $\tau_M$	Rheidity time, $\tau_R$
Soda-lime glass @ 250°C	25	$4.3 \times 10^{11}$	17 s	4.8 hr
Glacier ice @ 0°C	4	$\sim 10^{13}$	42 min	29 days
Halite @ 200°C	20	$3 \times 10^{16}$	17 days	48 yr
Earth mantle from glacial rebound	50	$10^{20}$	66 yr	66 000 yr

but it is obvious from glaciers that ice flows like a liquid over long timescales. Table 3.6 lists the Maxwell and rheidity times for a number of geologic materials.

Maxwell viscoelasticity neatly resolves other apparent paradoxes of earth science. William Thomson, later Lord Kelvin, used the difference between solid Earth tides and ocean tides to show that the Earth's elastic modulus is similar to that of steel. Kelvin himself, and Harold Jeffreys after him, never accepted the idea that over long intervals of time the Earth's mantle could flow like a liquid (England *et al.*, 2007). However, our modern understanding of mantle convection and plate tectonics requires just that. The resolution of this conundrum is through Maxwell viscoelasticity: Table 3.6 shows that the Earth's mantle (which is mainly composed of the mineral olivine) has a Maxwell time of about 100 years. Thus, the mantle behaves as an elastic solid with respect to the month-long tidal deformation (or even the 22-month Chandler wobble of its axis), and yet flows like a liquid during the 100 Myr timescale of mantle convection.

Ironically, Lord Kelvin himself provided one of the most graphic illustrations of the role of viscoelastic flow in the Earth and other planets. Kelvin loved mechanical models, often stating that he could "never satisfy myself until I can make a mechanical model of a thing" (Kargon and Achinstein, 1987). In his famous *Baltimore Lectures* of 1884, Kelvin described a classroom model in which he floated a layer of "Scottish shoemaker's wax" on a beaker of water. He submerged a number of corks underneath the wax and set a few lead bullets on top (Figure 3.8). Over the course of a semester, the bullets sank into the viscoelastic wax while the corks burrowed upward into it. By the semester's end, the bullets had dropped to the bottom of the beaker and the corks had emerged on top. While he could not have found a better analogy for the geologic behavior of the Earth, Kelvin himself used this model to illustrate his concept of the hypothetical aether, to show how the Earth could move through the all-pervading aether apparently without friction, while light waves traveled like elastic waves in this universal substance.

Maxwell's model of viscoelastic flow turns out to be only one of many possible variations. Depending upon how the elastic and viscous strains combine (coupled, more generally, with the possibility of plastic flow), a variety of viscoelastic (or elasto-viscoplastic) responses to stress are possible. Kelvin himself proposed a model in which elastic and viscous stresses are summed and the strains are then set equal. Now known as the



Figure 3.8 Lord Kelvin's class demonstration. Over the course of a semester, Kelvin showed that dense bullets would sink and light corks would rise through a layer of viscoelastic wax on top of a beaker of water. Although Kelvin himself did not intend it as such, it provides an apt illustration of the long-term flow properties of a planetary mantle.

Kelvin–Voigt model, it provides a better description of short-term flow, such as primary creep (the  $B$  term in Equation (3.27)), than does the Maxwell model (the  $C$  term in Equation (3.27)). The Kelvin–Voigt model may provide a good description of flow under short-term oscillatory stresses, such as tidal flexing, while the Maxwell model is more appropriate for steady, long-term deformation in which the total strain can increase without limit.

### 3.4.4 Planetary strength profiles

It should now be clear to the reader that the “strength” available to support topographical features on a planet is a complex issue. Topographic loads can be supported by the resistance to deformation exerted by cold solids, as well as by slow viscous or pseudoviscous deformation of warm solid materials. “Strength,” thus, depends on pressure, temperature, and the duration of the load, among many other modifying factors such as the pressure of included fluids, presence or absence of chemical weakening agents such as water, and even the history of previous deformation.

Given this complex response of “solid” materials to differential stresses, can one make *any* simple generalizations at all about the ability of planets to support topographical features? One simple observation is that strength generally decreases as temperature rises (and vanishes at the melting temperature). Most planets are warmer inside than on their outsides, although exceptions to even this apparently obvious situation occur during planetary accumulation and very large impact events. Thus, a simple generalization is that most of a planet's strength resides near its surface. This observation gives rise to the idea of a *lithosphere*, a relatively thin shell near the surface of planets large enough to have hot interiors, which embodies most of its long-term strength. The outermost part of the lithosphere is usually cool enough to exhibit brittle strength, while deeper portions resist loads by slow deformation (this definition of the lithosphere is oversimplified: It will be made more precise in the next chapter when the concept of Maxwell time is applied).

These ideas are used to construct *strength profiles*; envelopes that show the maximum differential stresses that can be supported as a function of depth in any given planet. Besides

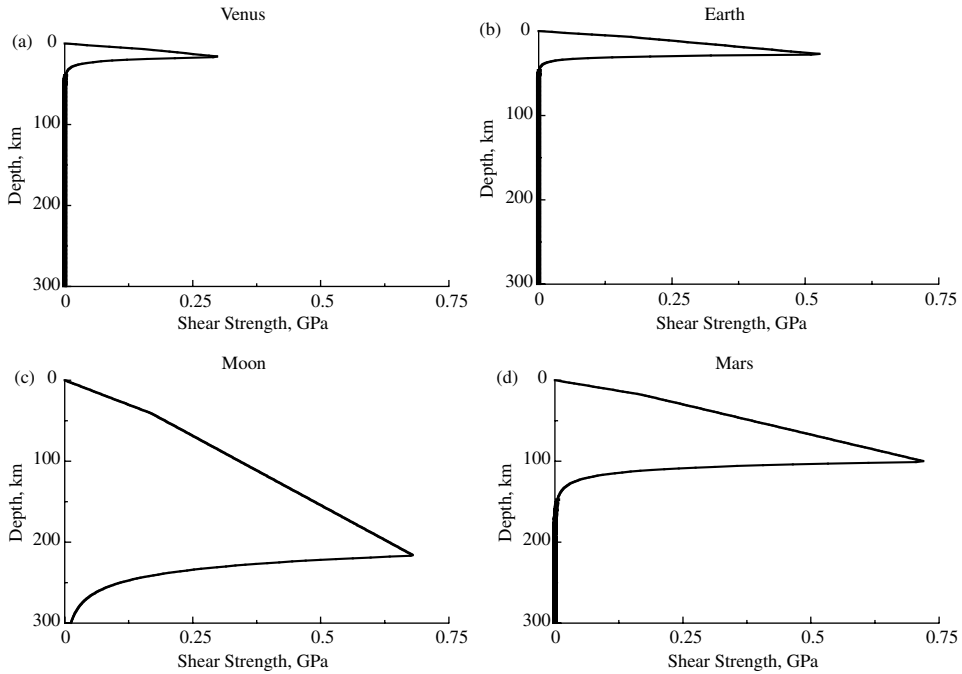


Figure 3.9 Strength profiles for the lithospheres of (a) Venus, (b) the Earth, (c) the Moon, and (d) Mars. The upper parts of the curve are controlled by friction on pre-existing fractures and, thus, follow Byerlee's law, Equation (3.25). The lower portions are cut off by creep in olivine, with parameters listed in Table 3.5. Temperatures are computed from mantle heat flow on the Earth and by assuming an average chondritic composition for the other planets. Thermal conductivity is taken to be 3.0 W/m-K. The strain rate is  $10^{-13} \text{ s}^{-1}$ , although the curves are only slightly different at  $10^{-15} \text{ s}^{-1}$ .

the failure laws themselves, these profiles require knowledge (or estimates) of the temperature and pressure as a function of depth. Because many factors influence strength, these curves are oversimplifications of the actual facts, and are useful only for general guidance to the strength levels available. There are also many variants of this kind of curve, each designed to show some especially pertinent relationship. To show the effect of strain rate, the strength profiles constructed here are assumed to reflect deformation at some particular strain rate. The cohesive strength of cold rocks is neglected because it is assumed that beyond some small strain the rock will fracture, so that only frictional strength continues to act.

Figure 3.9 shows computed strength profiles for Venus, the Earth, the Moon, and Mars. In all of these curves the upper cold portion is assumed to follow Byerlee's law, while the lower portion is controlled by the rheological properties of the common mantle mineral, olivine. Each assumes that the lithosphere is stretched at a strain rate of  $10^{-13} \text{ s}^{-1}$ , a typical plate-tectonic strain rate on the Earth. Very similar curves would result for lithospheric compression, with slightly higher frictional strengths. Lower strain rates decrease

the stresses in the lower part of the lithosphere and push the cusp marking the transition between friction and pseudoviscous flow to shallower depths. The sharpness of the cusp is artificial: In reality the transition is probably gradual, but the flow laws are not known well enough to represent this accurately.

The main lesson from these curves is that the maximum strength in a planet's interior resides neither at its surface, due to the pressure dependence of rock friction, nor at great depths, due to the weakening effect of high temperatures. The maximum strength is at an intermediate depth, and it is at this depth that most of the forces that support long-term topography are exerted.

### **3.5 Mechanisms of topographic support**

#### ***3.5.1 Plastic strength: Jeffreys' limit again***

Short-wavelength loads on a planetary lithosphere are supported by plastic strength, as described in Section 3.3.2. Stress differences reach approximately 1/3 of the vertical load and are supported at a depth comparable to the width of the load. The meaning of "short wavelength" is defined by reference to the thickness of the lithosphere. If the breadth of the load is comparable to or larger than the lithosphere's own thickness, then new factors come into play and more sophisticated models, such as the flexural models discussed later, in Section 3.5.5, must be brought into play. These new factors generally decrease the ability of the lithosphere to support the load: Jeffreys' theorem must always hold, but it does not guarantee that the stresses are not much larger than the minimum given by his limit. Direct support of a load by a strong material right underneath is always the most effective way to carry the weight of a topographic feature.

#### ***3.5.2 Viscous relaxation of topography***

Just as a mound created on the surface of a dish of honey gradually relaxes to a flat surface, so topographic features formed on the surface of a planet whose interior materials obey a viscous or pseudo-viscous flow law will eventually relax to a flat plain. Because of the complexity of the full non-linear pseudoviscous creep law determined for real rocks, most analyses of the viscous relaxation of topography approximate the actual flow law as Newtonian (at present, numerical methods are rapidly superseding such crude approximations, but there is still much to be learned from "back of the envelope" computations using Newtonian viscosity). The viscosity determined from such an analysis is then termed an "effective viscosity,"  $\eta_{\text{eff}}$ , and its value must be accompanied by an estimate of the stress at which it is determined. Although such a procedure is not exact, and in some special cases may be seriously misleading, it often yields useful insights into the mechanical behavior of a planetary body, so long as the user understands what the effective viscosity really is, and does not mistake it for what it is not.

Viscous relaxation acts to gradually erase any deviation from a “level” planetary surface (that is, from a surface coinciding with a gravitational equipotential surface). Thus, both elevations and depressions will gradually fade away with time. How much time this requires depends on the viscosity. If the viscosity is large enough, even a few billion years is not enough to erase the topography and we can speak of the surface elevations as “permanent,” even though, in principle, there is no such thing as a solid and all materials eventually creep to relax their deviatoric stresses.

The first estimates of the Earth’s viscosity derived from the early nineteenth-century observation by Swedish naturalist Celsius that some shorelines around the Baltic Sea are rising as rapidly as one meter per century. Hotly contested at the time, it is now accepted that central Scandinavia, formerly depressed by the weight of continental ice sheets, is gradually rebounding to its pre-ice age position. A still larger area in North America is currently rebounding from the former weight of the Laurentide ice sheets, which melted away about 11 000 yr ago. Although detailed analyses of the implications of this uplift have been ongoing for the past 60 yr, it is easy to perform a first-order estimate of the viscosity of the Earth’s interior that gives a value for its effective viscosity close to the most sophisticated modern determinations.

Following in the spirit of Jeffreys’ computation in Box 3.1, it is possible to balance the stress created by a depression (or elevation: the analysis is identical except for the sign) of time-dependent depth  $h(t)$  against the rate of deformation implied by the ideal viscous stress relation. Jeffreys’ theorem tells us that this stress difference is of order  $0.3\rho gh$ . The strain rate  $\dot{\epsilon}_x$  is of order  $\dot{h}/w$ , where  $w$  is the breadth of the depression. Inserting these factors into the definition of viscosity, Equation (3.12), yields a first-order differential equation for  $h(t)$ ,  $\dot{h}(t) = -[0.3 \rho ghw/\eta_{\text{eff}}]h(t)$ , whose solution is:

$$h(t) = h_0 \exp[-t / \tau_R]$$

$$\text{where } \tau_R = \frac{\eta_{\text{eff}}}{0.3 \rho g w}. \quad (3.34)$$

In this equation  $h_0$  is the initial depression due to the weight of the ice and  $\tau_R$  is the timescale for relaxation. It is this relaxation timescale that yields an estimate of the effective viscosity, which is thus given by:

$$\eta_{\text{eff}} = (0.3 \rho g w) \tau_R. \quad (3.35)$$

As one might intuitively expect, the relaxation time grows longer as the viscosity increases, and it decreases as the crustal density or gravity increases. Perhaps the least intuitive result is that the relaxation time depends inversely on the width of the load  $w$ . A physically intuitive way of appreciating this result is to realize that as  $w$  increases, the depth over which the flow occurs also increases. For a given pressure gradient, the flow is faster in a wider channel, leading to a faster relaxation rate. Thus, for a given viscosity, broad loads relax faster than narrow ones. The important implications of this result will shortly be highlighted in more detail.

In addition to the viscous half-space assumed in the relaxation computation just outlined, a second important limit is that of a thin viscous channel underlying the load. Following through a derivation similar to that above yields an equation similar to (3.34), except that the inverse load width  $1/w$  is replaced by  $w^2/d^3$ , where  $d$  is the depth of the thin channel (this derivation requires the equation for the parabolic velocity profile driven by a pressure gradient in a thin layer, a topic of so-called lubrication theory). In this case the relaxation time  $t_s$  is proportional to the load width, squared. A more general analysis of the relaxation of an axisymmetric crater of arbitrary profile on a substrate whose viscosity is a more complex function of depth can be found in Section 8.4 of Melosh (1989).

Performing an actual estimate of the viscosity beneath the Canadian shield, take  $2700 \text{ kg/m}^3$  as the average crustal density,  $9.8 \text{ m/s}^2$  as the acceleration of gravity, suppose the load is 3000 km across and that it relaxes over a timescale of 6000 yr. This yields an order-of-magnitude viscosity estimate of  $5 \times 10^{21} \text{ Pa-s}$ , nearly identical to the current best estimate for the Earth's lower mantle. To interpret this estimate, remember that most of the stress generated by a broad load is supported at a depth of about  $1/3$  the load width; that is, about 1000 km deep in this case, or near the top of the Earth's lower mantle. Furthermore, this is an effective viscosity that applies to a stress level of about  $0.3 \rho g h_0$  or around 20 MPa, assuming that  $h_0$  was about 2 km.

Although the idea of using the duration of topographic support to estimate planetary viscosity was first applied to the Earth, planetary geologists were quick to apply this idea to the planets. Ralph Baldwin, in his epochal 1963 book, *The Measure of the Moon*, made the first estimates of the Moon's viscosity based on the persistence of its non-hydrostatic tidal bulge and on the depths of lunar basins. In 1967 Ron F. Scott, a soil mechanics engineer at Caltech, was inspired to show how lunar surface viscosities could be estimated from the shape of relaxed lunar craters. He created a number of model crater shapes in a pan of viscous tar and allowed them to relax, recording how their shapes changed with time. Three of his time steps are shown in Figure 3.10. The most prominent characteristic of these changes is the dependence of relaxation rate on the size scale of the feature. Thus, large craters relax faster than small ones, so long as the viscous substrate is deeper than the diameter of the crater. Furthermore, the small-scale crater rims persist long after the larger-scale crater bowls have relaxed, just as Equation (3.34) suggests (other factors, such as the presence of a shallow lithosphere, may account for the persistence of crater rims on real planets, as opposed to craters in pans of uniform-viscosity tar).

Although Scott and others thus showed how viscous relaxation affects crater morphology, it has not yet been conclusively demonstrated that viscous relaxation has actually occurred in craters on any of the terrestrial planets or moons. Processes such as impact erosion or lava infilling often obscure any depth changes caused by viscous flow. The absence of relaxation does give useful lower limits to the viscosity, but this does not constitute a numerical measurement. However, the icy moons of the outer Solar System tell a different story. Figure 3.11 shows a 500 km wide crater, Odysseus, on the Saturnian satellite Tethys, contrasted with an unrelaxed 130 km wide crater, Herschel, on Mimas. Odysseus' floor has clearly relaxed to conform to the equipotential surface of the satellite, while its still-sharp

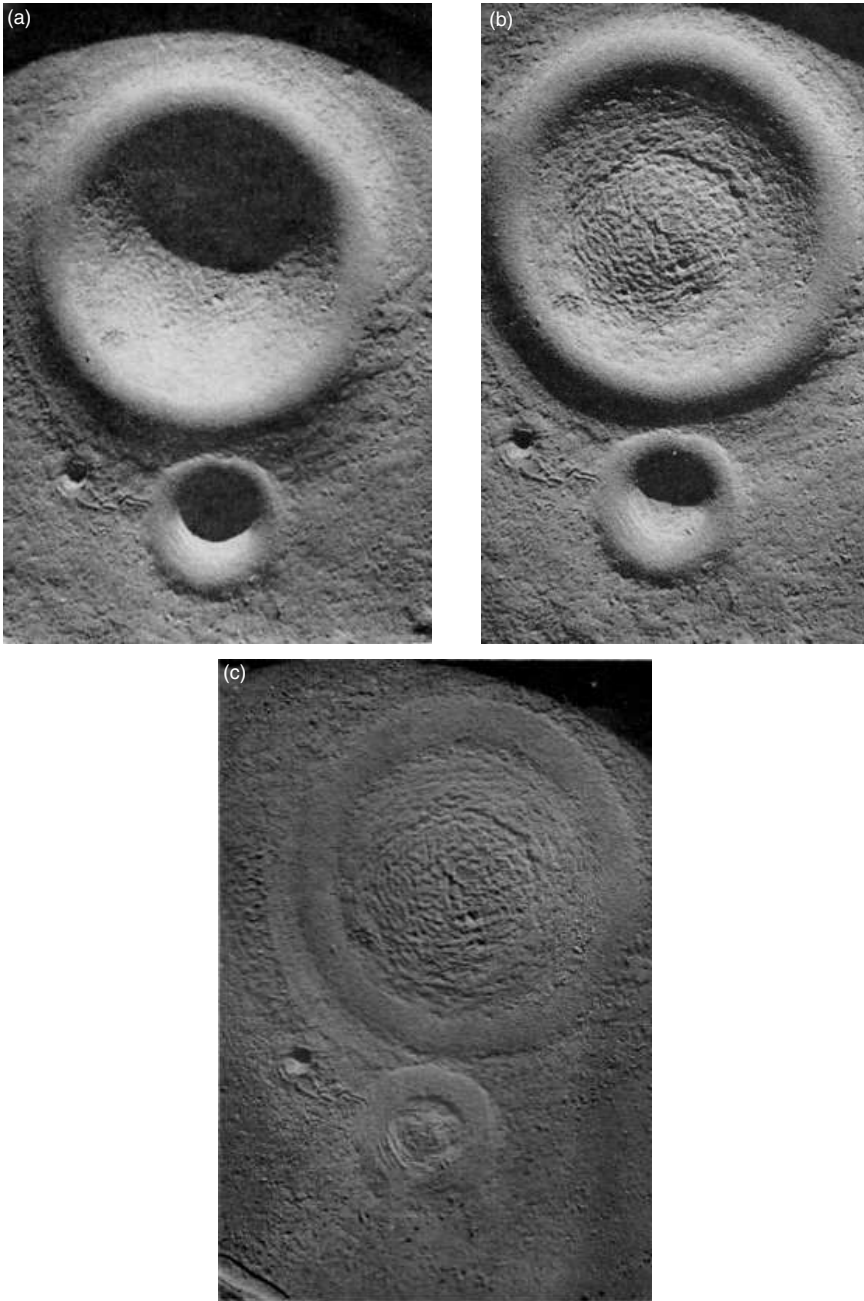


Figure 3.10 Viscous relaxation of model craters produced in asphalt of viscosity about  $10^5$  Pa-s. The largest crater is about 10 cm in diameter and the smaller craters about 2 and 0.2 cm. (a) 0.1 minute after the craters were molded into the surface. (b) After 30 minutes the larger crater floor has rebounded and the middle-sized crater floor is beginning to rise. All of the crater rims are still sharp. (c) After 18 hours the large and middle crater and their rims have relaxed, while the smallest crater is still evident. Image selection from Scott (1967).

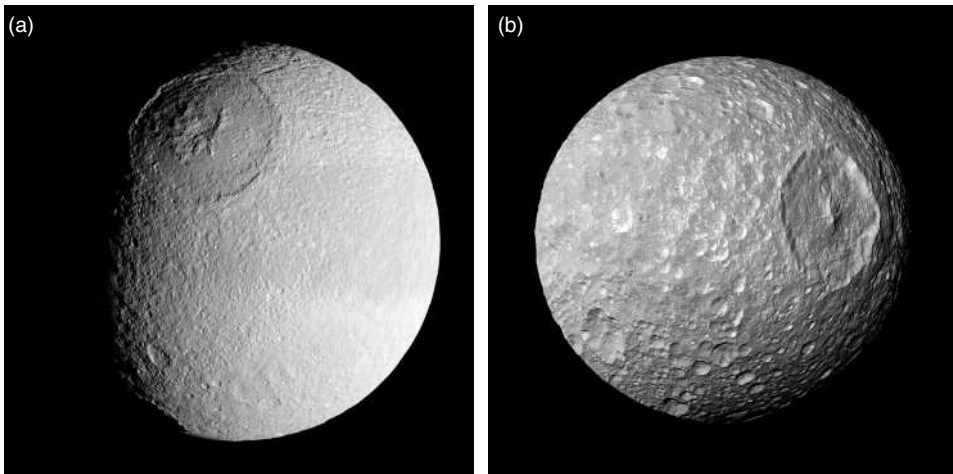


Figure 3.11 Large craters on moons of Saturn (a) The floor of the 500 km diameter crater Odysseus on Tethys has mostly relaxed to conform with the spherical shape of the satellite. NASA Cassini image PIA 08400. (b) The 130 km diameter crater Herschel on Mimas shows little sign of viscous relaxation. NASA Cassini image PIA 12570.

rim and central peak attest to the size-dependence of viscosity. If the age of the crater were known, these two observations would produce a tight bound on the viscosity of the moon, and by implication (from laboratory measurements of the flow law of ice) give an estimate of the internal temperature of Tethys. Much effort by planetary scientists is currently being expended on viscosity estimates of this kind, with the ultimate goal of estimating internal temperatures and even temperature gradients.

An important, but often overlooked, point refers back to Jeffreys' theorem: Topographic loads are typically supported at a depth comparable to the width of the load. Thus, the viscosity deduced from the relaxation of a feature of breadth  $w$  applies to a depth comparable to  $w$  itself (or, slightly better, about  $w/3$ , as indicated in Table 3.1). The fact that a narrow crater rim relaxes more slowly than the crater bowl itself is, thus, due to both the scale dependence of the relaxation time in Equation (3.34) and also to a possibly different (generally larger) viscosity at shallower depths below the narrow rim. In effect, topography of breadth  $w$  "probes" the viscosity at a depth of about  $w/3$ . When sufficiently detailed data on crater relaxation profiles are available this effect can be used to invert for the depth dependence of viscosity and, by inference from creep measurements on the (presumed known) underlying material, for the subsurface temperature gradient.

One of the major surprises of the past few decades is the existence of substantial topography on the planet Venus. Shortly after its 730 K surface temperature was discovered, but before its surface had been imaged by spacecraft-borne radar systems, material science expert J. Weertman (1979) predicted that any mountains on Venus would have long since relaxed away and that its surface must be a vast, gently undulating plain. On Earth, the temperature contour that defines the bottom of the elastic oceanic lithosphere is similar to

Venus' surface temperature, so this prediction seemed very reasonable. The discovery of large topographic variations on Venus, first by the Soviet Venera 15 and 16 radar missions and then by the US Magellan mission, was thus greeted with consternation. To this day we do not fully understand why the crust and upper mantle of Venus are so strong. The most common assumption is that high temperatures have cooked all of the water out of its near-surface rocks, thus eliminating the major weakening agent affecting terrestrial and Martian rocks. However, even the total elimination of water and the assumption of a low thermal gradient can barely explain the existence of the 13 km high Maxwell Montes, the highest elevation on Venus.

### 3.5.3 *The topographic advantages of density differences: isostatic support*

Most of the long-wavelength topography on the silicate planets and moons is a direct consequence of the difference in density between a crust and underlying mantle. Where no density differences exist, such as on the icy moons of Jupiter or Saturn, elevation differences tend to be of short wavelength. The resulting concept of *isostasy* has long been a staple of geological explanation on Earth. It has found broad application to the Earth-like planets. The basic idea of isostatic equilibrium is that high topography is high because it is underlain by rocks that are less dense than average. Elevation correlates with either density itself (Pratt isostasy) or with the thickness of a layer of lesser density (Airy isostasy). The crust is supposed to be in floating equilibrium, so that at some depth below the surface (the depth of isostatic compensation) the pressure of the overlying rock layers is the same along an equipotential surface.

A key component of the idea of isostatic equilibrium is that at the depth of isostatic compensation, deviatoric stresses vanish and pressure is the only force available. This concept accords well with the observational facts indicating that as the temperature rises, rock strength declines and creep rates increase. Initial stresses, even those applied nearly instantaneously by, say, the formation of an impact crater, relax rapidly on a geologic time-scale and bring topography into a state of isostatic equilibrium. This idea puts a premium on determining the depth of this level of compensation. If its depth can be determined, for example, using the methods discussed in the next section, this information can be converted to an estimate of the planet's interior temperature.

Geodesist Colonel George Everest accidentally initiated the discovery of isostasy in 1847, while he was triangulating the "Great Arc" in India. As he approached the massive Himalayan mountains he found that he could not get good agreement between his triangulated positions and astronomical measurements of latitude. J. H. Pratt, archdeacon of Calcutta, who was familiar with Newton's law of universal attraction, suggested that the mountains deflected the vertical, although the observed deflection was much less than what he first calculated. Pratt then supposed that the rocks underlying the Himalayas might be less dense than those underlying the Indian peninsula. Pratt announced his conclusions in 1855, the same year that G. B. Airy, the Astronomer Royal of Great Britain, suggested that variations in the thickness of a low-density crust floating on a denser substratum could account

for Everest's observations. Four years later Pratt published his own theory of isostasy in which he attributed variations in the elevation of surface features to lateral variations in the density of the crust above a level of "compensation," at which the density is uniform.

Geodetic observations in the late 1800s could not discriminate between the Pratt and Airy models. In the early twentieth century the US Coast and Geodetic survey officially adopted the Pratt model because of its computational simplicity, but when the developing field of seismology revealed deep roots beneath the Alps and Himalayas, the weight of opinion swung in favor of Airy isostasy for most of the twentieth century. Most recently, however, it has been shown that Pratt isostasy dominates California's southern Sierra Nevada. The elevation of the western US's Colorado Plateau now appears to be due to low densities in the mantle, not the crust. Furthermore, precise gravity measurements from the Magellan spacecraft have shown that the Pratt mechanism, with the low densities supplied by some combination of high temperature and a low-density mantle residuum, may support the volcanic uplands of Venus (Smrekar *et al.*, 1997). Evidently, the Pratt and Airy mechanisms are end members of a continuum and the determination of crustal and mantle density and thickness must be pursued independently, insofar as that is possible.

The application of the idea of isostasy to planetary topography is simple, which is part of its appeal. Figures 3.12a and 3.12b illustrate the idea of isostatic balance between two crustal columns in both the Pratt and Airy limits. For simplicity, these examples assume constant densities for both the crust and mantle, but it is easy to generalize these examples by integrating a depth-dependent density from the surface down to the depth of compensation.

For the Pratt hypothesis, Figure 3.12a, the pressure at the depth of compensation,  $d_c$ , beneath the plains and highlands crustal blocks is given by:

$$[\rho_{cp}t + \rho_m(d_c - t)]g = [\rho_{ch}(t + h_p) + \rho_m(d_c - t)]g \quad (3.36)$$

The contribution from the depth of compensation, as well as the mantle density and the acceleration of gravity all cancel out, so that the topographic elevation on the Pratt hypothesis,  $h_p$ , is given in terms of the crustal thickness below the plains,  $t$ , by:

$$h_p = \left( \frac{\rho_{cp} - \rho_{ch}}{\rho_{ch}} \right) t. \quad (3.37)$$

For the Airy hypothesis, Figure 3.12b, the density of the crust  $\rho_c$  is the same in both crustal columns, but the thicker crust sinks with respect to the thinner crust and produces a root beneath the highlands of thickness  $t_R$ . Performing the same type of pressure balance as for the Pratt case,

$$[\rho_c t + \rho_m(d_c - t)]g = [\rho_c(t + h_A + t_R) + \rho_m(d_c - t - t_R)]g. \quad (3.38)$$

Again benefiting from many cancellations, including the crustal thickness itself, the final expression for the elevation in terms of the depth of the root is:

$$h_A = \left( \frac{\rho_m - \rho_c}{\rho_c} \right) t_R. \quad (3.39)$$

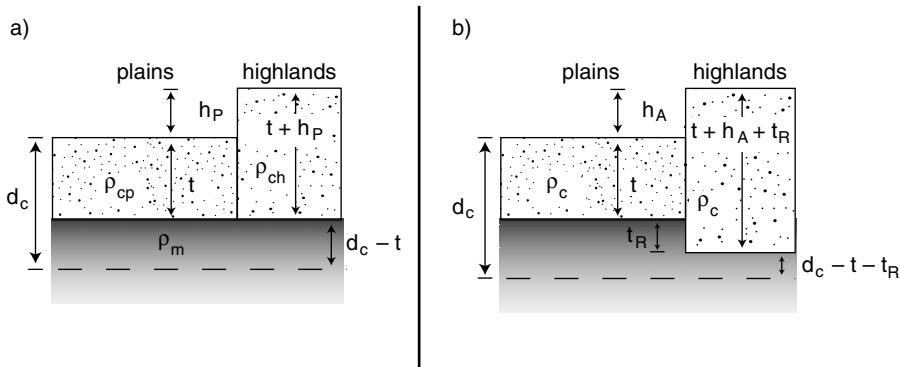


Figure 3.12 Isostatic compensation of topography is possible where a low-density crust overlies a higher-density mantle. (a) Pratt isostatic compensation, in which highlands are underlain by less dense crustal material than lowland plains. (b) Airy isostasy, in which the crust is the same density everywhere, but is thicker under highlands than plains. The dimensions defined in this figure are used in equations described in the text. The horizontal dashed line near the bottom of both figures is the depth of compensation, below which no stress differences are postulated to exist.

Because of these cancellations, the depth of isostatic compensation does not contribute directly to the topography for either Pratt or Airy isostasy. This is both a blessing and an annoyance: Insofar as the depth of compensation cannot be directly measured, we lose an important piece of information about the flow in a planet's interior. We must thus resort to indirect methods to learn about internal temperatures.

Isostatic equilibrium, although often assumed to be the final state of topographic relaxation in much of the geological literature, is not, in fact, the most stable end state: The minimum energy of any self-gravitating body is attained only when the density decreases monotonically outwards from the center of mass. Thus, even when the topography is fully compensated there is a tendency for low-density material to spread over adjacent denser rocks, and for mountain roots to spread laterally. Stress differences, thus, still exist in a state of full isostatic compensation. Calculation of these stress differences and their implications for flow in the crust of the Earth is now a part of terrestrial geodynamics (Sonder and Jones, 1999).

Although isostasy does contribute greatly to topographic support, it cannot evade the principal part of Jeffreys' theorem: Stresses of order  $\rho gh$  must still develop somewhere beneath the load. The advantage of the isostatic support mechanism is that it shifts the location of the maximum stress differences from a depth comparable to the width of the topographic load to the region above the depth of compensation, where the rocks are cooler, stronger and, thus, more capable of bearing the load. Vertical topographic loads are converted into horizontal loads acting near density or thickness gradients. It is even possible to convert topography into detailed horizontal stress maps, assuming that isostasy is strictly valid (Artyushkov, 1973; Fleitout and Froidevaux, 1982; Molnar and Lyon-Caen, 1988). Thus, planet-wide elevation differences, such as the hemispheric dichotomy of Mars or the

center of mass-center of figure offset of the Moon can be supported by modest stresses in the cooler, stronger outer layers of the planet, rather than by long-term strength at great depths.

### 3.5.4 Dynamic topography

Slow viscous or pseudoviscous deformation can do more than just eliminate pre-existing topographic features. Stresses generated by forced flow can actually create topography. When this occurs, the resulting elevations and depressions are referred to as *dynamic topography*. Slow flows in the interior of planets may be generated by a number of processes, but the most common are driven by density differences, where the density deviations from the mean are due either to temperature differences (the process is then referred to as thermal convection) or to compositional differences (compositional convection). The slow convective flows that drive plate tectonics in the Earth are a combination of both types of difference.

The most striking dynamic topographic features on the Earth are the deep submarine trenches that mark the sites of subduction zones. At subduction zones the cold, dense, and relatively stiff tectonic plates sink into the warmer, less dense mantle at rates up to about 10 cm/yr. As the plates sink, they undergo a sharp bend, changing their attitude from nearly level to plunging at angles that may exceed 45°. The cool, highly viscous material of the plates thus undergoes a large amount of stretching on the upper part of the bend, counterbalanced by compression at depth. This stretching creates stresses that literally suck the overlying surface downward, resulting in the observed topographic troughs. The depth of the trough is readily estimated from the definition of the effective viscosity, Equation (3.29), along with Jeffreys' theorem:

$$h_{\text{dynamic}} = \left[ \frac{\eta_{\text{eff}}}{0.3 \rho g} \right] \dot{\epsilon} = \left[ \frac{\eta_{\text{eff}}}{0.3 \rho g} \right] \frac{v}{w} \quad (3.40)$$

where  $v$  is the velocity of motion (subduction, in this case) and  $w$  is the distance scale over which bending occurs.

Unfortunately, we cannot accurately determine the effective viscosity from first principles, but we can invert the formula and determine how large it must be to give the observed ca. 5 km of trench depth as the plate bends through a radius  $w \sim 200$  km. The result, about  $2 \times 10^{21}$  Pa-s at a stress of about 50 MPa, is at least reasonable – it is almost two orders of magnitude greater than that of the underlying asthenosphere and in moderately good agreement with extrapolated laboratory measurements of the creep rate of olivine at this stress level.

One of the major complications in making this kind of estimate precise for subduction zones is that the much stiffer brittle-elastic plate that tops the tectonic plates interferes with the viscous flow deeper within the plate. Indeed, many models for subduction zones focus exclusively on the elastic plate and neglect viscous flow entirely. Such models, which were

among the earliest explanations of subduction zone topography, suffer from the prediction of enormous extensional stresses in the strongly bent elastic plate (up to 5 GPa, far in excess of any measured rock strength) and neglect seismic data that indicate that the elastic plate is extensively fractured and, thus, unlikely to support any extensional loads at all. Nevertheless, this kind of elastic-viscous coupling is common in planetary tectonics and will be discussed in more detail in the next chapter.

The other likely source of dynamic topography on the Earth (with its unique plate tectonics) and the other planets is associated with rising (or descending) convective plumes. Arising from deep within a planetary interior, buoyant plumes approach the surface and exert viscous stresses on the overlying cool rock layers. These stresses account for a substantial portion of the uplift associated with the plume's arrival (the rest is associated with the plume's low density). Equation (3.40) can also be used to estimate the dynamic portion of the topography associated with a plume of horizontal dimension  $w$  rising at a velocity  $v$ , provided an estimate of the effective viscosity can be made.

Because dynamic topography can develop even when temperatures are too high to permit much static rock strength, it has been suggested that a vigorous plume rising from deep within the Venusian mantle might cause the astonishingly high elevations of Maxwell Montes and Beta Regio on Venus. The estimated plume velocities must be quite high, on the order of meters per year, and if the flow fluctuates with time, one might expect to see the elevation of Maxwell Montes fluctuate in concert with the flow. Pursuing this idea, the Magellan radar altimeter repeatedly measured the height of Maxwell throughout the duration of the mission, seeking for measurable fluctuations. Unfortunately, none were found and the reason for Maxwell's high elevation remains unresolved.

### ***3.5.5 Floating elastic shells: flexural support of topographic loads***

A small, cool planet or moon may possess considerable long-term strength right down to its center. However, as interior temperatures rise, strength declines and the ability of a large planet to support long-duration, non-hydrostatic loads comes to reside exclusively near its surface. This gives rise to the concept of a lithosphere, a cool outer rind whose strength is controlled by increasing pressure near its top and by slow viscous creep near its base. The mechanical behavior of such a lithosphere can be very complex: Its upper portion responds to loads both by elastic deformation and plastic failure, while its underside flows on long timescales. However, a drastic but surprisingly effective approximation neglects the viscous deformation altogether and treats the lithosphere as an elastic plate floating on a perfectly fluid substratum. Loads on the surface flex the lithosphere downward and are supported by a combination of elastic stress from the lithosphere itself and the buoyancy of the displaced fluid below. The lithosphere thus supports loads in the same way that a skater on a frozen pond is supported by the flexure of the layer of ice. Indeed, Heinrich Hertz, otherwise renowned for his discovery of radio waves, first published the equations describing the effect of a point load on floating ice in 1884 and so initiated the mathematical study of lithospheric support.

Flexural models of topographic support were first proposed around 1900, when most scientists supposed that the interior of the Earth is literally molten and that the continents simply float on a liquid interior like ice on a frozen pond. Although it is now clear from the propagation of seismic shear waves and the slow rate of post-glacial rebound that the Earth's interior is actually a hot, viscoelastic solid, the relaxation of differential stresses at high temperatures still makes the elastic flexure approximation a good one for loads of long duration.

The bottom of the elastic lithosphere is now understood to be the depth at which the Maxwell time equals the duration of the load to be supported. Surface rocks behave elastically above this depth and flow gradually below it. Because the duration of the load enters into the lithosphere thickness, this concept is a bit fuzzy: For a load lasting only a few minutes, as might be applied by a meteorite impact, the entire mantle of the Earth is the lithosphere. For glacial rebound over 10 000 yr, the effective lithosphere is about 100 km thick, whereas for a mountain chain built over 100 Myr the lithosphere thickness might be only a few tens of kilometers. However, because the creep rate of most rocks is a strong function of temperature, the effective lithosphere thickness varies only by a small amount for loads lasting from a few million to a few billion years. Under these circumstances the lithosphere can be approximated as having a constant thickness determined by its composition and the near-surface thermal gradient.

The equations describing the response of such a floating elastic shell are very complex. In their simplest form, for a thin flat plate of uniform thickness, they obey a fourth-order partial differential equation called the biharmonic equation. However, these equations need not be solved to attain a qualitative idea of how topographic loads are supported by an elastic lithospheric shell. The most important concept deriving from these equations is embodied in a factor with dimensions of length called the *flexural parameter*,  $\alpha$ , which is defined as:

$$\alpha = \left[ \frac{1}{3(1-\nu^2)} \frac{Et^3}{\rho_m g} \right]^{1/4} \quad (3.41)$$

where  $t$  is the thickness of the lithosphere and  $\rho_m$  is the density of the mantle underlying the lithospheric plate.  $E$  is Young's elastic modulus,  $\nu$  is Poisson's ratio, and  $g$  is the acceleration of gravity. A representative value of  $\alpha$  for the Earth's oceanic lithosphere is about 53 km, derived from the deflection caused by the Great Meteor Seamount in the Atlantic Ocean (Watts *et al.*, 1975). It is generally a few times larger than the lithosphere thickness itself, which in this case is about 16 km.

The flexural parameter describes the tradeoff between elastic flexure and buoyancy in supporting a concentrated load. Loads of breadth smaller than the flexural parameter are mainly supported by elastic stresses that develop in the warped lithosphere, whereas broader loads must be supported by buoyancy; that is, by isostatic forces. Flexure thus fills the gap between topographic loads much narrower than the thickness of the lithosphere, which are supported essentially on an elastic half-space, and very broad topographic loads that are supported by isostasy.

There is, however, a price to be paid for the advantages of flexural support. Plate flexure creates bending stresses, and for broad loads these stresses are usually much larger than the minimum required by Jeffreys' theorem. In the absence of isostatic support, for a sinusoidal load of wavelength  $\lambda$  elastic plate flexure theory gives a maximum stress of:

$$\sigma_{\max} = \frac{3}{2\pi^2} \frac{\lambda^2}{t^2} \rho_c g h. \quad (3.42)$$

Thus, because of the factor  $\lambda/t$ , squared, stresses build rapidly when the width of the load becomes substantially broader than the plate thickness. This equation suggests that as the load breadth increases, the flexural stress increases without limit. However, this does not occur when a low-density crust overlies a denser mantle: At long wavelengths isostasy takes over and the stresses actually decline as  $1/\lambda^2$  after the stress peaks at a wavelength of  $\sqrt{2} \pi \alpha$ .

The surprisingly high stresses that develop in an elastically flexed plate are reduced somewhat when plastic yielding occurs and spreads the stresses over a larger volume, but the lesson is that flexure cannot support very broad loads. Indeed, in locations where the topography suggests that flexural support is important, it is common to observe tectonic evidence of rock failure.

The flexural parameter  $\alpha$  is often directly observable. The size of the region depressed by a concentrated load is governed by the flexural parameter. Thus, the island of Hawaii is surrounded by a broad shallow moat where the elastic lithosphere of the Pacific Ocean floor is flexed downward by the weight of the volcanic pile. Similarly, the ice shell of Europa is flexed downward by the weight of the ridges crisscrossing its surface, creating shallow troughs flanking the ridges (Figure 3.13). The gigantic Artemis Corona on Venus is partially surrounded by a moat similar to that around Hawaii, and also may be due to a flexing (or, perhaps, subducting and flexing) lithosphere.

One of the goals of planetary surface studies is to find evidence for such flexural depressions flanking topographic loads and, from their breadth, use Equation (3.41) to determine the thickness of the lithosphere. This thickness, in turn, can be used to estimate the near-surface temperature gradient, and, hence, planetary heat production.

### 3.6 Clues to topographic support

With all of the different mechanisms that can contribute to topographic support, the question naturally arises, how can we tell which mechanism, or what combination of mechanisms, is actually supporting the topography of a given planet? Some first-order guesses are easy: Long-wavelength loads are generally supported by isostasy, short-wavelength loads by flexure. Limits to the strength of materials provide some clues. However, how can we know, in a particular case, what mechanism is actually in play?

### Box 3.3 Flexure of a floating elastic layer

Determining the deformation of the surface of a floating elastic plate under a given load is both an old problem and a difficult one. Heinrich Hertz (of radio-wave fame) first offered a solution in 1884 (Hertz, 1884). His interest was not planetary lithospheres, but rather the form of the surface of a frozen pond under the weight of an ice skater. The weight of the skater (what we would now call a concentrated load) is supported both by the bending of the ice layer itself and by the buoyancy of the underlying water displaced by the deflection of the lower surface of the ice layer. Hertz's solution relied on centuries of mathematical study of the deflection of beams and the creation of an effective theory of elasticity. His work on the deflection of a floating plate found immediate application to railway engineering, where the bed of the tracks forms a support similar in many ways to a dense liquid layer.

In more recent times, the well-known geophysicist Don Anderson relates (personal communication, 1971) that his first introduction to plate tectonics took place courtesy of the United States Air Force, which required him to use Hertz's theory to determine how close together airplanes might be parked on an ice floe before the ice ruptured. Currently, the theory of plate flexure is widely applied in geodynamics to investigate the structure and evolution of planetary lithospheres. It is the principal subject of at least one modern monograph (Watts, 2001) and is discussed as part of thousands of papers on both terrestrial and planetary geophysics.

A serious student of terrestrial or planetary geophysics should, thus, be familiar with both the derivation and many applications of the flexural equations. However, the passage of time has not made this subject much easier than it was for Hertz, and a full derivation would be out of place in a broad overview (indeed, the correct application of the lower boundary condition between elastic and fluid materials presents a subtlety so obscure that, of all the books I know, only one (Cathles, 1975) treats it correctly!). The equations are, happily, linear for small vertical deflections  $w$  of the centerline of the plate. They are, however, *fourth-order* differential equations that, thus, have four parameters that must be determined from the boundary conditions. The most frequently used version of the full equations assumes that both the plate and the load are uniform in the  $y$  direction, hence, the solution depends only on the horizontal distance  $x$ :

$$D \frac{\partial^4 w}{\partial x^4} + N \frac{\partial^2 w}{\partial x^2} + \rho_a g w = q(x) \quad (\text{B3.3.1})$$

where  $N$  is a horizontal force applied in the  $x$  direction (taken to be positive in compression),  $\rho_a$  is the density of the underlying fluid layer,  $g$  is the acceleration of gravity and  $q$  is an applied surface load (force per unit area).  $D$  is the flexural rigidity, defined in terms of the Young's modulus  $E$ , Poisson's ratio  $\nu$  and plate thickness  $t$  as:

$$D = \frac{E t^3}{12(1 - \nu^2)}. \quad (\text{B3.3.2})$$

A typical solution to this equation is given by Figure B3.3.1, which shows the deflection of the lithosphere under a load of uniform thickness  $a$  that extends arbitrarily far to the left of the center,  $x = 0$  and infinitely far perpendicular to the page. This might represent the edge of a very broad plateau with a straight edge. The density of both the load and the flexed plate is  $\rho_p$ , while that of the underlying fluid layer is  $\rho_a$ . The formula for the vertical deflection of the *center of the lithosphere* in this case is:

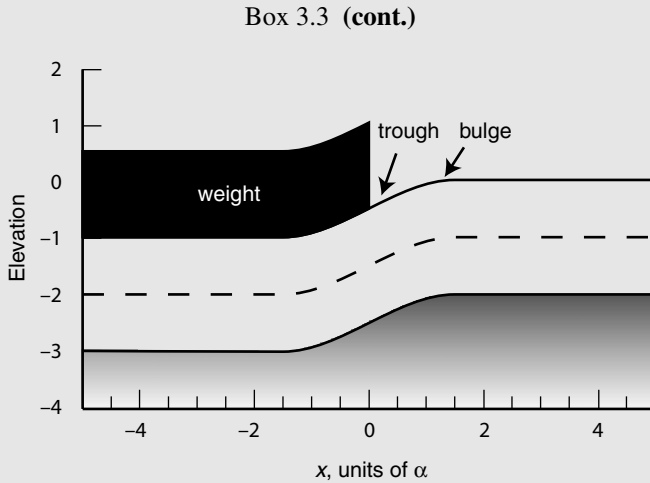


Figure B3.3.1 Deflection of a floating elastic plate by a sharp-edged load with the same density as the plate. The horizontal dimension is in units of the flexural parameter  $\alpha$ , while the elevation is in units of half of the lithosphere thickness. The dashed line is the neutral sheet of the plate. The load uniformly depresses the plate on the left, but near the edge of the load the plate is flexed down with a curvature comparable to the flexural parameter. A very low bulge develops beyond the main flexure. Equation (B3.4.3) in Box 3.3 describes the deflection of the neutral sheet.

$$w(x) = \begin{cases} \frac{\rho_l}{\rho_a} \frac{a}{2} \{2 - e^{x/\alpha} \cos(x/\alpha)\} & x \leq 0 \\ \frac{\rho_l}{\rho_a} \frac{a}{2} e^{-x/\alpha} \cos(x/\alpha) & x > 0. \end{cases} \quad (\text{B3.3.3})$$

In these equations the horizontal scale of the deflection is determined by the flexural parameter,  $\alpha$ , defined in the text. To find the actual topography one must be careful to add in the thickness of the overlying half of the plate, plus the load. The lithosphere is deflected downward by a distance of  $\frac{\rho_l}{\rho_a} \frac{a}{2}$  right under the edge of the load, while far to the left it achieves the deflection required by isostatic equilibrium,  $\frac{\rho_l}{\rho_a} a$ .

Note, in Figure B3.3.1, the very slight reversal of the vertical deflection that crests at a distance of  $3\pi\alpha/4$  (labeled “bulge” in the figure). Noted by Hertz in his solution, this small-amplitude reverse deflection is characteristic of flexural solutions. On Earth, this slight bulge is readily apparent on topographic maps of the great oceanic trenches where the oceanic lithosphere is subducted into the mantle. A few hundred kilometers seaward of every trench there is a small rise, termed the “outer rise,” that seems to represent the flexure of the oceanic lithosphere. The flexural trough surrounding each of the Hawaiian islands is likewise accompanied by a slight outer rise farther from the island loads.

The above results are valid only for a flat elastic plate. When the lithosphere has a substantial curvature it is technically called a shell and the solutions for topographic support must include membrane stresses from the stretching or compression of the plate in addition to flexural stresses. This case is examined in some detail by Turcotte *et al.* (1981).

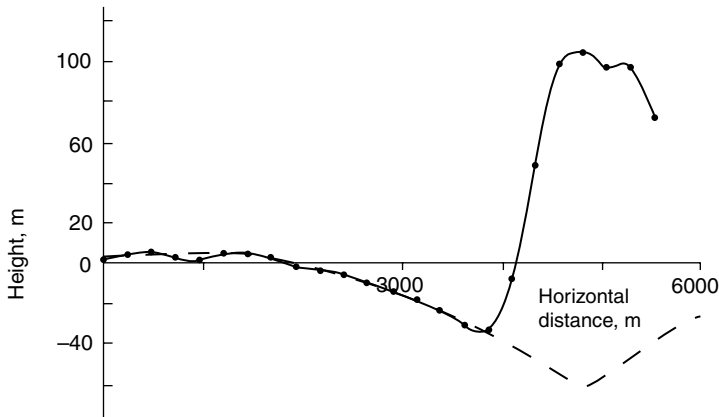


Figure 3.13 Flexure of the lithosphere adjacent to a ridge on Europa. The plot shows the topography determined by the method of photoclinometry applied to a Galileo image of Europa. Note the prominent trough flanking the ridge and the low bulge beyond the trough. This trough and bulge topography is the expected shape for a loaded floating elastic plate of thickness  $350 \pm 50$  m. After Figure 4 in Hurford *et al.* (2005).

This question would be easy to answer if we could directly determine the stresses acting in a planet's interior. Unfortunately, stresses are difficult to measure even in the laboratory. *In situ* stress measurement techniques do exist, however, and are sometimes used at shallow depths in the Earth (Engelder, 1993), but such data do not yet exist for any other planet. Earthquakes also give clues about stress magnitudes and directions, but even in the Earth their interpretation is presently somewhat controversial, and for other planets the necessary seismic data sets do not exist (apart from some intriguing, but limited-term, data on lunar seismicity). Associations of tectonic features, to be discussed in more detail in the next chapter, may give clues about regional stress distributions and this is an important source of information. However, the most direct information on topographic support comes from measurements of the acceleration of gravity.

### 3.6.1 Flexural profiles

The most direct method of determining lithospheric thickness is to observe a topographic flexural profile. As discussed above, such profiles are commonly observed around volcanic islands in the Earth's oceans (Fig 3.14), and have been noted on Venus and Europa. Figure 3.13 is a good example of such a profile, first discovered in 2005 (Hurford *et al.*, 2005). Upon observing new images of the surface of a terrestrial planet or satellite, one of the first efforts of any geophysically oriented planetary scientist is to seek evidence of such surface deformation. Once found, the wavelength of the observed topographic flexure is readily expressed in terms of the flexural parameter  $\alpha$ , Equation (3.41), and with a few additional assumptions it yields the thickness of the elastic lithosphere. Still more assumptions give an estimate of the planet's heat flow, a number that is difficult to determine remotely in almost any other way. The amplitude of the flexural deflection yields the magnitude of the load via the full flexural equations described in Box 3.3.

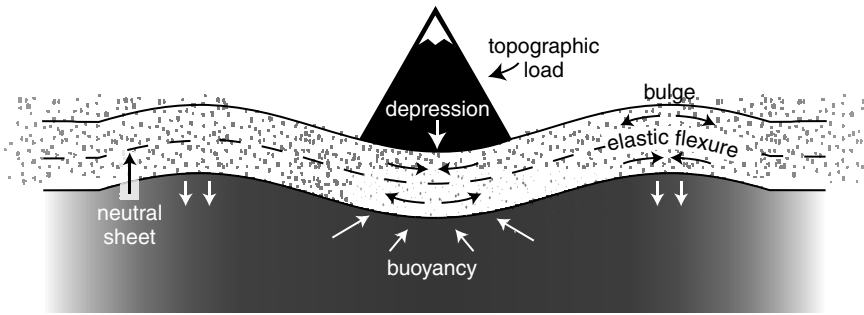


Figure 3.14 Flexure of a floating elastic plate subjected to a topographic load. The weight of the load is supported by a combination of flexural stresses developed by bending of the plate and buoyancy generated by the depression of the lithosphere into the fluid mantle below. This schematic drawing indicates the neutral sheet in the plate by a dashed line.

### 3.6.2 Anomalies in the acceleration of gravity

To first order, the gravitational acceleration of a large planet or satellite is directed toward its center of mass and varies as the inverse square of the distance from that center, outside of the body itself. However, small but significant deviations from an ideal spheroidal field (for a rotating body) are readily detected either on the surface or from orbiting satellites. This is not the place for a detailed discussion of this large area of research (see, e.g. Lambeck, 1988), but a few important results require brief discussion.

Deviations of the gravitational acceleration of a body from an ideal assumed field are known as *anomalies*. Free-air anomalies are probably the easiest to understand: they are simply the difference between the expected gravitational acceleration and the observed acceleration at some conventional elevation above the surface. Gravity anomalies are generally reported in units of *gal* (short for galileo: 1 gal = 1 cm/s<sup>2</sup>). The excess gravitational acceleration produced by an infinitely wide sheet of density  $\rho$  and thickness  $h$  is given by:

$$\Delta g = 2\pi G\rho h. \quad (3.43)$$

Thus, the gravitational acceleration exerted by a broad sheet of basalt 1 km thick is about 125 mGal. Although this is a very small acceleration compared with the surface acceleration of the Earth (9.8 m/s<sup>2</sup>, or 980 000 mGal), such anomalies are readily detected by the orbital perturbations of low-flying satellites. Indeed, accuracies of 0.1 mGal are presently achievable.

The importance of free-air gravity anomalies is that, to first order, isostatically compensated topography has no anomaly. Because the extra mass of surface topography is compensated by a low density at depth, the net excess mass below the surface of isostatically compensated topography is zero, and so is the gravity anomaly. This simple conclusion is not quite true for loads of limited lateral extent, in which case detailed modeling is required, but it works as a general rule of thumb. Topography supported by strength in the form of flexure or supported dynamically is not compensated by underlying low densities

and so exhibits free-air gravity anomalies, which may be quite substantial. For example, free-air gravity anomalies over the dynamic topography of subduction zone trenches may drop below  $-300$  mGal. Flanked by smaller positive anomalies along the volcanic arc, they constitute the largest free-air gravity anomalies on Earth.

Anomalies in the acceleration of gravity (both excesses and deficits) can be interpreted as equivalent topographic loads (positive or negative) and, thus, sources of stress in the lithosphere. A rough-and-ready method of estimating such stresses is to replace the gravity anomaly,  $\Delta g$ , by a broad layer of sufficient mass to create the same anomaly, then to equate the weight of this extra load to the applied stress. This yields an equation for the equivalent stress  $\sigma_{\text{grav}}$  of the gravity anomaly:

$$\sigma_{\text{grav}} = \frac{g \Delta g}{2 \pi G} \quad (3.44)$$

where  $G$  is Newton's gravitational constant. In the case of the 300 mGal anomalies observed in terrestrial oceanic trenches, this corresponds to a stress of about 70 MPa – close to the crushing strength of rock. On the moon, the same anomaly would only imply a stress of about 12 MPa: Although the mass anomaly is the same on the moon, its lower acceleration of gravity implies a smaller stress.

An important episode in the history of lunar exploration was the unexpected (and, at the time, unwelcome!) discovery of strong mass concentrations on the lunar nearside. Termed “mascons” after they were discovered in 1968, they are circular anomalies of up to about 500 mGal that are associated with basalt-filled impact basins. The Apollo mission planners went to great trouble to compensate for the effects of these anomalies in the manned Apollo orbits. The mascons' effect on satellite orbits is so strong that they crashed the Apollo 16 subsatellite PFS-2 onto the lunar surface only a month after the astronauts released it.

It is now understood that isostatically uncompensated lava within the circular nearside impact basins creates most of the mascon anomalies, with an additional contribution from an uplifted mantle plug underneath the basins (Neumann *et al.*, 1996). The effect of the lava's enormous weight is clearly visible in the Humorum basin, where adjacent craters tilt inward toward the sagging basin center and the stresses generated by the load have fractured the crust in great circumferential faults.

A second commonly employed type of gravity anomaly is the Bouguer anomaly. It is computed from the free-air anomaly by subtracting an estimate of the gravitational attraction of the topography above (or below) the reference geoid. The resulting anomaly reflects the mass deficit (or excess) below (or above) the topographic elevation (or depression). For more details on this and other types of gravity anomaly, see the book by Garland (1965). Isostatically compensated mountainous terrain, such as the Alps in Europe, exhibits small free-air anomalies and strong negative Bouguer anomalies, reflecting the low-density root compensating the weight of the mountains. If it is further assumed that the density anomalies are entirely due to variations in the thickness of a constant-density crust, then gravity anomalies can be inverted to create maps of crustal thickness. Such maps have been

produced for the Earth, Moon, and Mars, but it should be understood that a great many assumptions enter into such maps unless they are constrained by seismic data.

Because isostatic compensation by a floating lithosphere depends on the breadth of the load, a useful approach is to compute the Fourier transforms of both gravity anomalies and topography. Comparison of the amplitude of the gravity anomaly to topographic height as a function of wavelength on a so-called admittance diagram may then be used to estimate the thickness of the elastic lithosphere. Unfortunately, subsurface loads easily confuse this method; more recent work focuses on correlations between gravity anomalies and topography as a function of wavelength. This kind of study yields maps of lithosphere thickness, which have been compiled to date for the Earth, Venus, and Mars.

### 3.6.3 Geoid anomalies

A somewhat different type of gravity anomaly is the ratio between geoid height and topographic elevation (or depression). The geoid, by definition, coincides with a gravitational equipotential surface, whereas the acceleration of gravity is proportional to the potential gradient perpendicular to this surface. The geoid and gravitational acceleration anomalies, thus, contain different types of information. It can be shown that geoid height variations depend on the near-surface density *gradient*, rather than the density itself. Thus, the Geoid to Topography Ratio, or GTR, allows estimates of the depth of isostatic compensation as well as of the type of compensation, whether of the Airy, Pratt, or mixed type.

Over the Earth's oceans the geoid can be measured directly by precision observations of the shape of the sea surface. Over the land areas of the Earth and over planets with solid surfaces it can be constructed from careful tracking of gravitational perturbations of satellite orbits.

The geoid of Mars is utterly dominated by the huge Tharsis dome, which affects a region about 5000 km in diameter and appears to overlie an enormous lens of low-density material in the Martian mantle. Because of the uncompensated load, the Tharsis dome causes such a large geoid distortion that it obscures efforts to determine that planet's moment of inertia and thus the size and mass of its core (Neumann *et al.*, 2004). On Venus the GTR of highland features is much larger (tens of m/km; Smrekar *et al.*, 1997) than those of terrestrial features (typically less than 5 m/km in the oceans). These large ratios indicate much larger depths of isostatic compensation than observed on the Earth (a paradox, considering the much thinner lithosphere on Venus because of its high surface temperature!). Furthermore, the GTR varies widely from one highland feature to another, suggesting a highly variable depth of compensation. The major geoid anomalies on Earth are associated with subduction zones. However, unlike the acceleration anomalies, which are negative in the trenches and positive over the flanking volcanic arcs, the geoid anomalies are broad positive welts that follow the trend of the subduction zones. These anomalies are generally attributed to the cold, dense subducted slabs slowly sinking into the mantle.

The great importance of gravity anomalies for understanding topographic support is the principal reason that planetary geophysicists are eager to establish polar orbiters about as many planets and satellites as possible. The Earth, Venus, and Mars have been well covered

### Box 3.4 The ambiguous “lithosphere”

The term “lithosphere,” as introduced in this chapter, refers to that part of a planet’s interior that responds elastically to applied loads. Because of the time-dependent response of rock materials to applied stress, the lithosphere’s size and location is somewhat ill defined, as it depends on the duration of the load under consideration and the rheology of the material of which it is composed. It is, nevertheless, a useful concept because the extreme variations in the effective viscosity of most planetary materials make the uncertainties in the lithosphere’s boundaries small in relation to the size of the elastic region itself for timescales of geologic duration.

However, the ambiguities of the term “lithosphere” only begin with this definition. Numerous geophysicists over the past 70 years have complained that the same term is promiscuously applied to three disparate concepts (Anderson, 1995), but to little avail: The word “lithosphere” is employed by large segments of the geophysical community to mean either the elastic portion of a planet’s interior (the “elastic lithosphere”), the portion of the Earth above the seismic low-velocity zone (the “seismic lithosphere”), or the cold boundary layer of a thermally convecting cell (the “thermal lithosphere”). It is wise to be cautious when encountering the term “lithosphere” and to ask oneself which usage is intended!

Another frequent confusion is between “lithosphere” and “crust.” The outer regions of planets are frequently differentiated into an outer, less dense crust that overlies a deeper interior zone often called the “mantle,” in analogy to the divisions of the Earth’s interior. The distinction between the crust and mantle is purely chemical: They are composed of materials with different average densities. In contrast, the elastic lithosphere is a mechanical division. In the Earth’s ocean basins, the elastic lithosphere comprises *both* the oceanic crust and upper mantle, while on the continents the elastic lithosphere may include only the upper portion of the crust (and this is often underlain by a *second* lithosphere at the top of the mantle).

by such orbiters. Our Moon is not so well understood because we cannot directly measure the range to a satellite over its farside. High-precision lunar gravity measurements of the farside will require missions that incorporate at least two satellites tracking one another. Recently, the successful Japanese Kaguya mission has produced the best and most complete lunar gravity field, including the farside. At the time of writing, the MESSENGER mission is on its way to orbit Mercury in 2012 and we are eagerly awaiting the data on Mercurian gravity that will result from successful completion of that mission. In the future we can hope for missions that orbit, and track, spacecraft around the major moons in the outer Solar System.

### Further reading

G. K. Gilbert achieved a great deal of insight into the relationship between temporary loads on the Earth’s surface and the viscous response of the underlying mantle in his famous monograph on Lake Bonneville (Gilbert, 1890), which can still be read with profit. The history of the investigation of the strength of the Earth and gravity anomalies,

among other things, is well told by Greene (1982). Long a classic in the field, the book *Fundamentals of Rock Mechanics* by J. C. Jaeger has gone through many editions. It was out of print for many years, but a new edition has recently appeared that updates its notation and includes many new measurements (Jaeger *et al.*, 2007). The ideas behind our modern understanding of material strength are engagingly told in a semi-popular book (Gordon, 2006), while the details of brittle fracture theory are explored by Lawn and Wilshaw (1993) and for rocks by Paterson and Wong (2005). The nature and theory of dislocations is well described in Hull and Bacon (2001) and Weertman and Weertman (1992). Gilman (1969) applies dislocation mechanics to the plastic deformation of solids. Harold Jeffreys devoted much of his life to understanding the relation between strength and topography of the Earth. He wrote a fine, although now somewhat dated, popular book (Jeffreys, 1950), but his enduring masterpieces are the third and fourth editions of *The Earth* (Jeffreys, 1952, 1962). Later editions of this book exist, but by the fifth edition, the aging Jeffreys was on a campaign to stamp out the upstart theory of plate tectonics and these later editions are rather polemic. The best treatment of the relation between gravity, the geoid, and the shape of the Earth is Lambeck (1988). A clear, detailed discussion of rheology applied to the Earth is Ranalli (1995), although a more recent book focused on the detailed mechanisms of deformation and flow is Karato (2008). The now-classic book on the application of theories of elasticity and viscosity to geodynamic problems is Turcotte and Schubert (2002). This book has become a standard text for advanced courses in geodynamics. The flexure of the lithosphere and its relation to isostatic support is now well covered at book length by Watts (2001).

## Exercises

### 3.1 Strength vs. gravity

- a) Phobos, the innermost satellite of Mars, is an irregular, potato-shaped body with extremes of radius,  $r_{\min} \approx 10$  km and  $r_{\max} \approx 14$  km, and mean density  $1900 \text{ kg/m}^3$ . If these extremes are the maximum that Phobos' strength could support, how large is the strength of its rock? If the strength of Phobos' rock is similar to that of the Moon's, about 10 MPa, how large could the extremes of Phobos' radii be? What do you think this means?
- b) If asteroids are incoherent "rubble piles", the maximum slope that can exist on their surface is the angle of repose for rock debris, about  $30^\circ$  for most types of rock. Estimate the *maximum* difference in elevations possible on a non-rotating rubble-pile asteroid and compare this to the actual difference in dimensions of known asteroids.

Extra Credit: Suppose the asteroid is rotating at the limit for breakup. Now estimate (crudely: to do this exactly is a *very* hard problem) the maximum possible difference in the asteroid's dimensions. For a more sophisticated approach to this problem see Minton (2008).

### 3.2 Viscous flow

Use the formula, similar to the one derived in Section 3.5.2, for the relaxation time  $\tau$  of a disk-shaped load on a viscous half-space with viscosity  $\eta$ :

$$\tau = 5\eta/\rho gR$$

where  $\rho$  is the rock density,  $g$  is the surface acceleration of gravity, and  $R$  is the radius of the disk.

- The Imbrium mascon ( $R = 500$  km) is not isostatically compensated (relaxed). The last lavas on its surface are ca.  $3 \times 10^9$  yr old. Derive a lower limit for the Moon's present-day viscosity.
- Lake Bonneville (Ancestral Great Salt Lake in Utah) relaxed almost completely in the 1500-year interval between the Bonneville and Provo stages, when much of its water drained out to the northern Columbia River drainage. Its radius  $R \approx 100$  km. What is the viscosity of the mantle beneath Utah? Compare this to the viscosity ( $10^{21}$  Pa-s) of the average mantle. What does this mean?
- Over the last  $3 \times 10^9$  yr (probably), 100 km diameter crater basins on Ganymede have relaxed completely, but their 10 km wide rims are still clearly visible. What does this imply about the viscosity of Ganymede? Is there more than one possible interpretation?

### 3.3 Warmed-over Uranian moons

Tiny Miranda, radius 236 km and surface temperature about 70 K, has a shape that is indistinguishable from that of an equilibrium tidal ellipsoid, with a maximum tidal bulge of about 7.1 km. Using the fact that Miranda must have relaxed into this shape over the past  $4.5 \times 10^9$  yr, derive an upper limit for the viscosity of its interior (you may need to know  $G = 6.67 \times 10^{-11}$  Nm<sup>2</sup>/kg<sup>2</sup> and the mean density of Miranda is 1200 kg/m<sup>3</sup>).

### 3.4 The ultimate limit to core formation

Use Frenkel's estimate of the ultimate strength of a solid,  $Y_F = \mu/2\pi$ , to estimate the maximum radius,  $r_{\max}$ , of an iron sphere that can be supported in the Earth's mantle. Some relevant data are  $\rho(\text{iron}) = 8000$  kg/m<sup>3</sup> (at mantle pressures),  $\rho(\text{mantle}) = 5000$  kg/m<sup>3</sup>, and  $\mu = 2.5 \times 10^{11}$  Pa.

Reference (consult this *after* you have solved the problem!): G. F. Davies (1982).

### 3.5 Global isostasy

- Suppose that the Moon's center of mass (CM) is 1.6 km closer to the Earth than its center of figure (CF), as was determined by the Clementine mission. Model the Moon's interior as a mantle of density 3300 kg/m<sup>3</sup> and a crust of density 2800 kg/m<sup>3</sup>. If the crustal thickness on the nearside is 60 km (determined by the Apollo seismic experiment), how thick must the farside crust be to explain the CM–CF offset?

- b) Another way to estimate the Moon's crustal thickness is to note that the floor of the gigantic, 2600 km diameter, South Pole-Aitken basin lies about 8 km below the best-fitting sphere representing the lunar mean elevation. If we make the reasonable assumption that this impact cleared away *all* of the overlying crust, leaving bare mantle on the floor of the basin, use isostasy to estimate the Moon's mean crustal thickness. If this answer differs from (a) above, what may be the reason?

### 3.6 Supporting Maxwell

Maxwell Montes is the highest elevation on Venus, rising 11 km above the planet's mean radius and extending over a 500 km diameter region. It is possible that Maxwell is supported dynamically by viscous stresses induced by a rising mantle plume impinging on the overlying lithosphere. If this is correct, use order-of-magnitude estimates to deduce the *velocity* of the plume necessary to support Maxwell. You may assume the mean viscosity of the mantle is  $10^{19}$  Pa-s, similar to the Earth's asthenosphere. If this velocity fluctuates by 10% over the year that Magellan observed the altitude of Maxwell's summit, how large would the variations in elevation be? Do you think these elevation changes would be detectable?

### 3.7 Flexed Venustian lithosphere

The northern edge of Ishtar Terra on Venus is an enormous scarp, 4 km high, that stands near  $30^\circ$ , the angle of repose. Just north of the plateau edge is a deep trough that is bounded still farther away by a low rise that crests about 50 km away from the deepest part of the trough. Use the theory of a sharp-edged load on a floating elastic plate to estimate the Venustian elastic lithosphere thickness. How does this agree with other estimates of lithosphere thickness?

You may need to recall that the acceleration of gravity on Venus is  $8.6 \text{ m/s}^2$ , and may assume that the elastic constants of the Venustian crust are approximated by  $E = 1.6 \times 10^{11}$  Pa and  $\nu = 0.25$ .